The Pearcey function and the cusp catastrophe

The Pearcey function and the cusp catastrophe

D.A.MacBeath, B.Sc.

A Thesis Submitted to the School of Graduate Studies in Partial Fulfilment of the Requirements for
the Degree of Master of Science

August 31, 2016

MASTER OF SCIENCE (2016) McMaster University
(Physics) Hamilton, Ontario

TITLE: The Pearcey function and the cusp catastrophe
AUTHOR: D.A.MacBeath, B.Sc.
SUPERVISOR: Professor D.W.L.Sprung
NUMBER OF PAGES: vi, 45

Abstract

The subject of this work is a theoretical analysis of the Pearcey function. In optics, thin lens theory supposes that all rays focus at a unique point where the field converges. For a real lens, the focal point is replaced by a cusp, which is the end point of a caustic curve dividing the bright field region from the dark. My particular interest is the pattern of nodal points within the cusp. By investigating the stationary points for the cusp catastrophe, asymptotic approximations are found for the Pearcey function. This in turn leads to the development of finding the positions of nodal points inside, and outside a caustic. Also values for $|P|$ on a small circle surrounding a node are examined and show reasonable accuracy of order 10^{-8}.

Acknowledgements

I would like to thank the following people and organisations for helping me complete this work:

- Department of Physics and Astronomy for TA and scholarships,
- NSERC for finance and support under discovery grant 3198,
- Dr. D.W.L Sprung for his guidance,
- Dr. D. O'Dell and Dr. W. Van Dijk for their assistance and enthusiastic discussion,
- Dr. G.V. Morozov for getting me here.

Contents

1 Introduction **1**

2 Catastrophe Theory **3**
2.1 Zeeman Catastrophe Machine 5
2.2 Cusp Catastrophe 7
2.3 Mapping 8
2.4 Structural stability and Codimension 9
2.5 Link to Geometrical Optics 11
2.6 Lens 12

3 Analysis of the Pearcey function **15**
3.1 Approximate solutions to the Pearcey function 15
3.2 Taylor Series method for small values of R 17
3.3 Method of stationary phase 19
3.4 Systematic method to find the nodal points 27
3.5 Zeroth Order 30
3.6 Line of nodes outside the caustic 35
3.7 Number and density of nodes below caustic 40

4 Conclusion **45**

A Plots of $|P|$ and phase P from Stamnes and Spjelkavik [1] **49**

List of Figures

2.1 Cusp Pattern via a reflective mirror. 5
2.2 Caustic with potentials 8
2.3 Equilibrium Surface and Control Space 9
2.4 Six rays are shown for various heights of h for only upper half of the lens; the lens is symmetric about the z-axis. Refractive index of $n = 1.5$ and thickness $t = 1.5$. Each surface has a radius of $R = 9$ units. . . . 13

3.1 Path of steepest descent 21
3.2 Paths of constant phase in complex u plane. Contours are inclined asymptotically at an of angle $\pi/8$ relative to the real/imaginary axes. The three branches pass through the three stationary points on the real axis. The contours pass through the stationary points u_1 and u_3 at an angle of $\pi/4$, whilst u_2 is traversed at an angle of $-\pi/4$. 24
3.3 $|P(-x, y)|$ on a circle of radius 10^{-7} around a node with a cosine curve for comparison. 25
3.4 $|P(-x, y)|$ on a circle of radius 10^{-8}. 25
3.5 $|P(-x, y)|$ on a circle of radius 10^{-9}. 26
3.6 Values of $|P|$ on a square grid around an approximate node. Contour lines are projected onto the zero plane. One unit of x and y corresponds to 5×10^{-9}. 27
3.7 Location of the nodes inside the caustic are presented here with (k, j) indexing labels. 34
3.8 Location of 10 nodes outside the caustic. 39
3.9 Approximately 400 nodes plotted vs $R = x^{3/2}$ and $\tilde{y} = y(3/2)^{3/2}$. . . . 42
3.10 Approximately 1200 nodes plotted vs $R = x^{3/2}$ and $\tilde{y} = y(3/2)^{3/2}$. . . 43
3.11 Nodes inside the caustic with modified axes $\tilde{x} = x^{3/2}$ and $\tilde{y} = y(3/2)^{3/2}$ 44

A.1 Contour lines of constant $|P(x, y)|$ of the Pearcey function. The dashed curve is the caustic. $|P(x, y)|$ has a maximum value of 2.64 at $x \approx -2.2$, $y = 0$. The contour lines are separated by equal intervals of 0.2, and the dotted side of each contour line indicates the direction of descent. 50

A.2 Contour lines of constant phase of the Pearcey function $P(x, y)$. The dashed curve is the caustic. The contours are labelled $a = \pm 180°$ and from $b = -150°$ to $l = 150°$ in steps of 30°. 50

Chapter 1

Introduction

In 1946 Pearcey [2] published the first detailed calculation of the EM field structure near the focus of a spherical lens located at $x \to -\infty$. This result is now known as the Pearcey function. This function takes the form of the second catastrophe known as the cusp in Thom's catastrophe theory. Physically the Pearcey function describes a brightly lit region of light bounded by a caustic, separated from a dark region outside. The cusp is useful for describing equilibrium positions and stability of dynamic systems such as boats or oil-rigs [3]. The Pearcey function has been used to predict elastic scattering or atomic collision [4], [5]. The propagation of electromagnetic waves in the ionosphere [6] has seen its use. Also in the novel study of Pearcey beams, which show interesting behaviour such as form-invariance on propagation and self-healing [7].

As light propagates through a medium it tends to focus not at a single focal point but rather across multiple foci. As a family of rays concentrates into a region of space, the boundary is known as a caustic. One of the initial problems in analysing caustics is that in the domain of geometrical optics, as you approach the caustic the intensity is non-physical and approaches infinity, due to the rays having no finite size. The other is that caustics were thought to be perturbed focal points due to aberrations in the medium. However they have been found to fit in a family of mathematical objects known as catastrophes.

Catastrophe theory was developed by Rene Thom in the 1960's. He classified seven elementary types of catastrophe patterns. Catastrophe theory is used to describe discontinuities and when applied to physical problems, it can describe the properties of a discontinuity without invoking specific details of the underlying mechanism. Each catastrophe corresponds to a different diffraction pattern with its own characteristic function. These functions can be related to polynomials within an integral. Set in some coordinate system, short-wave asymptotic solutions can be developed to satisfy the wave equation. In general one writes,

$$\psi(a) = \int_{-\infty}^{\infty} e^{iV(a,t)} dt$$

where a is a set of parameters and t is a variable of integration. The catastrophe of interest to me is known as the cusp. It can be described by the function, $P(x, y)$, known as Pearcey's function. I will outline the work of Kaminsky and Paris who found a method to locate the nodal points in a systematic way, with accuracy of $\pm 1\%$ or better.

Chapter two is devoted to a brief overview of catastrophe theory. The basics of catastrophe theory and the link to geometrical optics are explained.

Next, chapter three compares the various asymptotic approximations to the Pearcey integral by exploring the work of Stamnes and Spjelkavik [1], Kaminsky and Paris [8], and investigates the accuracy of such asymptotic analyses.

Chapter 2

Catastrophe Theory

René Thom developed his ideas in the 1960's and published *"Stabilité Structurelle et Morphogenèse"* [9] in 1972. Since then, the subject of catastrophe theory has developed considerably. Catastrophe theory is a topological model of a dynamical system, which stresses the importance of structural stability, where a system can be perturbed by a small amount while its behaviour remains locally unchanged. However, repeatedly disturbing the system by small perturbations may eventually cause the system to undergo a discontinuity. Thom devised a system whereby knowing the number of control variables, one may know the configuration of the discontinuity. If there are no more than four control variables, there are only seven distinct types of catastrophes. One of the catastrophes describes a caustic as an envelope of rays on a two-dimensional surface. The Airy function describes the intensity of a point caustic and the phase has the form of the fold catastrophe,

$$Ai(a) = \frac{1}{2\pi}\int_0^\infty e^{i(ax+x^3/3)}dx. \tag{2.1}$$

The Airy function is a well studied function which is related to a classical turning point of a quantum particle. An oscillating wave in one dimension approaches a caustic from $-\infty < a < 0$ and decays exponentially once it passes the caustic, positioned at $a = 0$, along the real a-axis. It is at a caustic where the wave goes from a having a bright intensity to a quickly decaying, dark region. The Pearcey function is a generalised version of the Airy function, but instead of it being in one dimension, a, the Pearcey function is in two, x and y. The seven elementary catastrophes are presented below. The first potential function in catastrophe theory is the fold which is assigned the standard form,

$$V_1 = x^3 + ax. \tag{2.2}$$

The second is the cusp catastrophe,

$$V_2 = x^4 + ax^2 + bx. \tag{2.3}$$

The third is called the swallowtail catastrophe

$$V_3 = x^5 + ax^3 + bx^2 + cx. \tag{2.4}$$

Following this, the butterfly,

$$V_4 = x^6 + ax^4 + bx^3 + cx^2 + dx. \tag{2.5}$$

then the hyperbolic umbilic catastrophe

$$V_5 = x^3 + y^3 + axy + bx + cy. \tag{2.6}$$

The elliptic umbilic catastrophe,

$$V_6 = \frac{x^3}{3} - xy^2 + a(x^2 + y^2) + bx + cy, \tag{2.7}$$

and finally the parabolic umbilic catastrophe,

$$V_7 = x^2y + y^4 + ax^2 + by^2 + cx + dy. \tag{2.8}$$

In all of these, x, y are variables of integration; a, b, c, d are control parameters. This chapter will outline the development and basic principles of Thom's theory concerning the cusp catastrophe.

The cusp catastrophe corresponds to the optical phenomenon known as a caustic. These can form in many scenarios, one being rays striking a cylindrical reflector. The intensity of the brightly lit region is large but knowing the shape and position of the pattern is sufficient for some analysis. In Fig 2.1 one can see rays travelling to the right impinging upon the cylindrical surface. The incident ray strikes the surface at θ_i and is reflected with an equal value of θ, measured from the normal between the incident ray and surface. These reflected rays do not converge toward one focal point but rather create a pattern of overlapping rays. The equation for a reflected ray, from Poston and Stewart [10], is given as

$$(y - \sin\theta)\cos(2\theta) = (x - \cos\theta)\sin 2\theta. \tag{2.9}$$

To find the equation for the cusp pattern produced by the mirror, differentiate Eq (2.9) with respect to θ and solve for x and y.

$$\begin{aligned} x &= \cos\theta - \frac{1}{2}\cos\theta\cos 2\theta \\ y &= \sin\theta - \frac{1}{2}\cos\theta\sin 2\theta \end{aligned} \tag{2.10}$$

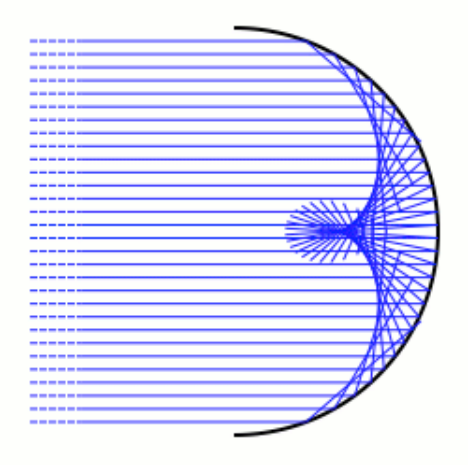

Figure 2.1: Cusp Pattern via a reflective mirror.

2.1 Zeeman Catastrophe Machine

A mechanical example of catastrophe is provided by Zeeman's machine. Invented in 1969 by E.C.Zeeman [11] the simple apparatus makes use of two rubber bands, some pins and a wheel put together in such a way that at certain points $P(\alpha, \beta)$ the machine will seek out minima via a discontinuous change in position. It should be noted that the parameters are changed smoothly as possible so as to represent a continuous change.

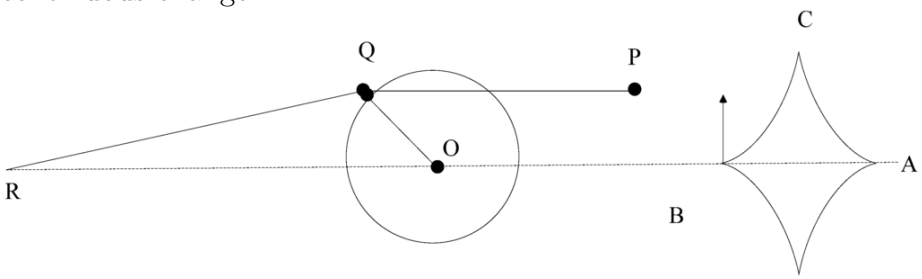

The above illustration depicts the Zeeman machine. A wheel is placed flat against a board and centred by a pin O, around which it can rotate. RQ and QP represent the two rubber bands, at Q both rubber bands are attached and fixed onto the edge of the wheel. RQ is fixed by another pin at point R, which is in line with OA, and QP is free at point P. To operate this device the free end of QP, P, is manipulated by a user in the plane of the device.

When P is outside of the cusp region (A, B, C), there is only one minimum for the potential, as P moves smoothly, the equilibrium of potential also changes smoothly. But inside the cusp there are two potential minima. As P enters the cusp, travels

smoothly across the symmetry line of AB and exits the cusp on the other side, the system undergoes an abrupt change where the orientation of the wheel jumps to a new position with a negative θ (which is the angle ROQ) all due to a smooth change of variables. This abrupt discontinuity of position is known as a catastrophe.

The potential energy of this system is a function of angle θ. According to Hooke's Law the potential energy of a stretched rubber band is proportional to the square of the stretch $(l - l_0)^2$. Setting $l_0 = 1$, we can write

$$V_{\alpha,\beta}(\theta) = \frac{\mu}{2}[(l_1 - 1)^2 + (l_2 - 1)^2] \tag{2.11}$$

where μ is the modulus of elasticity, l_1 is the length RQ and l_2 is the length QP. The lengths are defined in terms of θ and l_2 moves in (α, β) ,

$$l_1 = \sqrt{(2 - \frac{1}{2}\cos\theta)^2 + (\frac{1}{2}\sin\theta)^2}$$

$$l_2 = \sqrt{(d + \frac{1}{2}\cos\theta - \alpha)^2 + (\frac{1}{2}\sin\theta + \beta)^2}$$

where d is the length OB and θ is the angle ROQ.

By expanding $\cos\theta$, $\sin\theta$ in powers of θ the energy $V_{\alpha,\beta}$ takes the truncated form

$$V_{\alpha,\beta}(\theta) \approx \frac{\mu}{2}\left(a_0 + a_1\beta\theta + a_2\alpha\theta^2 + a_3\beta\theta^3 + a_4\theta^4 + \mathcal{O}(\theta^5)\right). \tag{2.12}$$

$a_0, \ldots, a_4$ are constants. We can take units where $\frac{\mu}{2}a_4 = 1$ to simplify the expansion, also for simplification the $\mathcal{O}(\theta^5)$ term may be omitted. The potential can then be written as,

$$V(\theta) \approx a_0 + a_1\beta\theta + a_2\alpha\theta^2 + a_3\beta\theta^3 + \theta^4$$

By shifting the origin of θ to $t = \theta + a_3\beta/4a_4$, one can get rid of the cubic term and rewrite the potential as

$$V(t) = at + \frac{1}{2}bt^2 + \frac{1}{4}t^4. \tag{2.13}$$

with $a = \frac{9}{5}\alpha$, $b = \frac{4}{3}\beta$.

Equation (2.13) is known as the standard form of the cusp catastrophe. In order to get some useful information about the cusp catastrophe, the critical points (i.e. the maxima and minima) of V must be analysed.

2.2 Cusp Catastrophe

Here is the Pearcey function with the cusp in the phase as described in Eq. (2.13).

$$P(a,b) = \int_{-\infty}^{\infty} e^{i(at+bt^2/2+t^4/4)}dt \tag{2.14}$$

This section deals with the analysis of the critical points of the cusp catastrophe. The critical points are given by taking the derivative of Eq.(2.13) with respect to t. This makes V into an extremum as the points where V is insensitive to small displacements is of interest. If you integrate along the real t-axis the integral oscillates infinitely rapidly due to the e^{it^4} factor.

$$\frac{dV(t)}{dt} = a + bt + t^3 = 0, \tag{2.15}$$

where a, b are real. This takes the form of a cubic and its characteristics are determined by the determinant,

$$D = 8a^3 + 27b^2. \tag{2.16}$$

- If $D > 0$, then there is one real root and a pair of complex conjugate roots.
- If $D = 0$, then all three roots are real but two coincide, i.e., if $a = b = 0$ then all three real roots coincide, but if $a \neq 0$ or $b \neq 0$ then only two of the roots coincide.
- If $D < 0$, then there are three real roots.

The nature of the roots depends entirely on the values of the parameters a, b, which are known as the *control parameters*, relative to the caustic. The caustic is plotted in Fig. 2.2. For chosen points the potential is plotted alongside them. The caustic is defined here as

$$8a^3 + 27b^2 = 0 \tag{2.17}$$

and using Eq. (2.17), it is shown that outside of the caustic there is one minimum and inside the caustic there are two minima.

This explains the discontinuous jumping of the wheel, as inside there are two positions for the wheel to be oriented and be in a local minimum, whereas outside there is only one and therefore the wheel must orientate itself to satisfy that single minimum. The curved lines are a cartoon of the potential energy of the Zeeman machine.

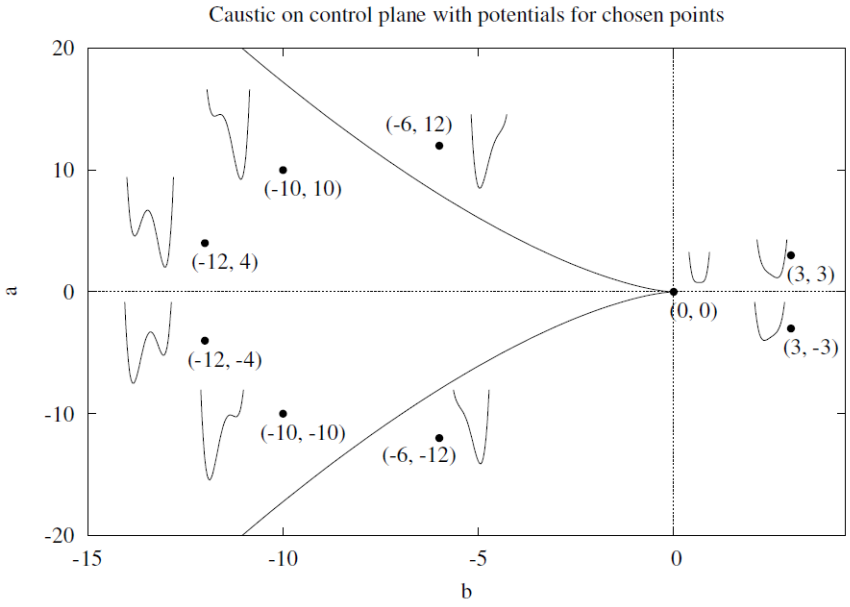

Figure 2.2: Caustic with potentials

Fig.2.2 is plotted in the a, b plane and the potentials are plotted as $V(t)$ vs t, the axes are left out, in order to view these potentials with greater ease. Going from near the centre line at $(-12, 0)$ inside the cusp there are two deep minima and as you approach the edge of the cusp, one of the potential minima's reduces in depth until outside, at $(-6, 12)$, it entirely disappears.

2.3 Mapping

An illustrative example of the discontinuity occurring over the caustic is shown when plotted in three dimensions. For simplicity to plot in *Maple* the equation is now stated as

$$V(x) = \frac{1}{3}xy - x^2z + x^4 \tag{2.18}$$

Dividing Eq.(2.18) by x and change the sign so as to have the orientation of the surface facing in a way that the overlapping feature is obviously present and finally the last term, y, involves a scaling factor of a third.

$$\frac{V(x)}{x} = \frac{1}{3}y - xz + x^3 \tag{2.19}$$

The caustic bifurcation set is also plotted on the y, z base plane.

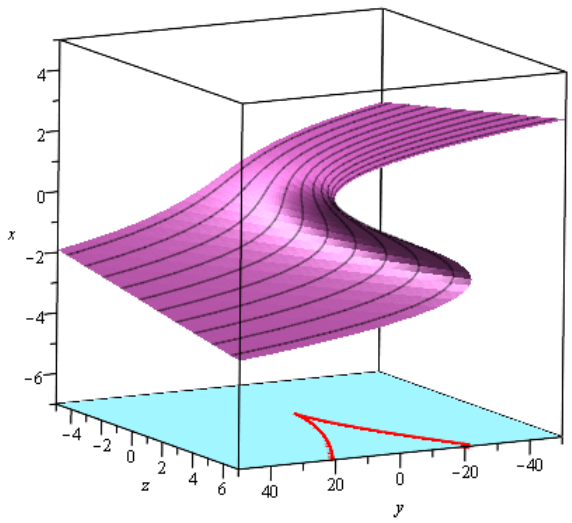

Figure 2.3: Equilibrium Surface and Control Space

The phase point lies on either the lower sheet or upper sheet in Fig. 2.3, since the middle sheet corresponds to unstable equilibria. The system point is located on the purple surface, and moves position as the control variables (z, y) are changed. Smooth variations in z, y almost always produce smooth variation in x except at the points highlighted by the caustic. The caustic $8x^2 + 27y^2 = 0$ is the red line projected onto the blue plane which represents the boundary of the folds. If the point system crosses the path highlighted by the caustic it must undergo a sudden change in x, that is, it jumps to the other sheet.

2.4 Structural stability and Codimension

An important aspect running in the background of catastrophe theory is the notion of structural stability. This section summarises the topic from Saunders. [12]. Suppose that $f(x)$ is a function of an m-parameter family of functions. If the parameters change continuously, then in this m-dimensional space the function may be represented as $f_a(x)$ for a point A. Another point, say B, is represented by a function of the same form, $f_b(x)$; if it is close enough to point A then $f_a(x)$ is called structurally stable. On the other hand, the set of all points A where these two functions are not stable is the called the bifurcation set.

The concern of this project is to investigate a two parameter function $P(x, y)$. In this subsection the splitting lemma will be developed for a two variable potential and

it will be shown that the number of essential variables can be reduced to one so as to ease the investigation. Let $f(x, y)$ be a smooth function in x and y with a critical point at the origin. That is, both x and y derivatives vanish.

$$f_x(0,0) = f_y(0,0) = 0. \tag{2.20}$$

Here $f_x(0,0)$ and $f_y(0,0)$ represent the partial derivatives with respect to x and y respectively. Expanding via the Taylor series

$$f(x,y) \approx \frac{1}{2}\left(\frac{\partial^2 f}{\partial x^2}x^2 + 2\frac{\partial^2 f}{\partial x \partial y}xy + \frac{\partial^2 f}{\partial y^2}y^2\right) + \text{higher order terms} \tag{2.21}$$

The determinant,

$$\Delta = \frac{\partial^2 f}{\partial x^2}\frac{\partial^2 f}{\partial y^2} - \left(\frac{\partial^2 f}{\partial x \partial y}\right)^2 \tag{2.22}$$

determines the type of critical point of the function $f(x, y)$,

$$\begin{aligned} \Delta > 0, \qquad & \frac{\partial^2 f}{\partial x^2} < 0, \quad \textit{maximum} \\ \Delta > 0, \qquad & \frac{\partial^2 f}{\partial x^2} > 0, \quad \textit{minimum} \\ & \Delta < 0, \quad \textit{saddle.} \end{aligned} \tag{2.23}$$

For functions with a large number of variables, these conditions can be expressed in terms of a matrix. Let $f(x_1, x_2, .., x_n)$ be a function of n independent variables with a critical point at the origin. Define a matrix, known as the Hessian,

$$H = \begin{bmatrix} \frac{\partial^2 f}{\partial x_1^2} & \frac{\partial^2 f}{\partial x_1 \partial x_2} & \frac{\partial^2 f}{\partial x_1 \partial x_3} & .... & \frac{\partial^2 f}{\partial x_1 x_n} \\ \frac{\partial^2 f}{\partial x_2 \partial x_1} & \frac{\partial^2 f}{\partial x_2^2} & \frac{\partial^2 f}{\partial x_2 \partial x_3} & .... & \frac{\partial^2 f}{\partial x_2 x_n} \\ .... & .... & .... & .... & .... \\ \frac{\partial^2 f}{\partial x_n \partial x_1} & \frac{\partial^2 f}{\partial x_n \partial x_2} & \frac{\partial^2 f}{\partial x_n \partial x_3} & .... & \frac{\partial^2 f}{\partial x_n^2} \end{bmatrix}. \tag{2.24}$$

If $\det H \neq 0$ then it is possible for a coordinate transformation to exist which lets one express f as

$$f = e_1 x_1^2 + e_2 x_2^2 + ... + e_n x_n^2 + \text{higher powers.} \tag{2.25}$$

where $e_i = \pm 1$. This shows that the rank of the Hessian is n if the determinant does not vanish. Now if the rank is dictated by a value of $n - r$, where r is a positive value then by similar logic of transforming the coordinates, the function may be written as

$$f = e_{r+1} x_{r+1}^2 + e_{r+2} x_{r+2}^2 + ... + e_n x_n^2 + \text{higher powers} \tag{2.26}$$

This is structurally unstable but it is defined by $x_1, x_2, ...x_n$ variables, which means that it can be studied by the r variables alone thereby reducing the number of variables having to be considered. In other words, variables ranging from

$$x_{r+1}, x_{r+2}, ...x_n$$

are inessential to the analysis and can be ignored and variables ranging over

$$x_1, x_2, ...x_r$$

are essential and describe everything that is necessary. This is the Splitting Lemma. The number of different types of catastrophes depends only on the number of essential state variables r and not on the number of state variables n. r is known as the co-rank of the Hessian.

2.5 Link to Geometrical Optics

A well-known link from geometrical optics to wave theory is shown by using the eikonal equation. Fermat's Principle is used, which states that a ray travels the shortest distance between two points.

$$\int_a^b n(x, y, z)\, ds = \min. \tag{2.27}$$

ds is the line element for the ray between two points a,b. The line element undergoes of change of variables, $x' = dx/dz$ and $y' = dy/dz$ so the integrand can be integrated by dz,i.e.

$$ds = \sqrt{dx^2 + dy^2 + dz^2} = \sqrt{1 + x'^2 + y'^2}\, dz.$$

Now Eq.(2.27) can be written as,

$$\int_a^b L(x, y, x', y')\, dz = \min, \tag{2.28}$$

where the Lagrangian is $L(x, y, x', y') = n(x, y, z)\sqrt{1 + x'^2 + y'^2}$. Eq (2.28) is minimised by solving the Euler-Lagrangian equations,

$$\frac{d}{dz}\frac{\partial L}{\partial x'} - \frac{\partial L}{\partial x} = 0 \tag{2.29}$$

$$\frac{d}{dz}\frac{\partial L}{\partial y'} - \frac{\partial L}{\partial y} = 0. \tag{2.30}$$

Substituting the Lagrangian into the above equations Eqs. (2.29) and Eq(2.30), one obtains

$$\frac{d}{dz}\frac{nx'}{\sqrt{1+x'^2+y'^2}} = \sqrt{1+x'^2+y'^2}\,\frac{\partial n}{\partial x} \tag{2.31}$$

$$\frac{d}{dz}\frac{ny'}{\sqrt{1+x'^2+y'^2}} = \sqrt{1+x'^2+y'^2}\,\frac{\partial n}{\partial y}\ . \tag{2.32}$$

Tidying these equations up by using the previous expression for ds

$$\left(\frac{d}{ds}\left[n\frac{dx}{ds}\right], \frac{d}{ds}\left[n\frac{dy}{ds}\right]\right) = \left(\frac{\partial n}{\partial x}, \frac{\partial n}{\partial y}\right)\ . \tag{2.33}$$

This is approximately the eikonal equation for a ray vector

$$\frac{d}{ds}\left(n(\vec{r},\omega)\frac{d\vec{r}}{ds}\right) = \nabla n(\vec{r},\omega). \tag{2.34}$$

2.6 Lens

This section will explain how to trace rays through a symmetric spherical lens and shows a geometric optics interpretation of a catastrophe. To start of with, consider an spherical lens with thickness $2t$. The lens is in the z, y plane and has symmetry about the z-axis. Each face of the lens is an arc centred at $z = \pm R \mp t$, where R is the radius of a circle. Imagine a family of incident rays running parallel to the z-axis approaching the lens from left hand side, passing through the lens at different heights relative to the surface. These rays impinge on the surface and travel through the lens cause multiple focal points to build up and therefore will create bright regions, ending in a cusp.

A ray at height h impinges on the lens at point z_a and the angle of the ray from the normal to the lens is $\sin(\theta_0) = h/R$. At point z_a,

$$\begin{aligned} h^2 + (z_a - R + t)^2 &= R^2 \\ h^2 + (z_a + t)^2 - 2R(z_a + t) &= 0 \\ (z_a + t) = R - \sqrt{R^2 - h^2} &\approx \frac{h^2}{2R} \end{aligned} \tag{2.35}$$

After the ray passes through the first surface at an angle of θ_0 to the normal it will enter at an angle of θ_1, specifically $\sin\theta_1 = \frac{1}{n}\sin\theta_0$, until it meets the second surface of the lens. The ray will meet the second surface of the lens at point z_b at a height denoted by h_b above the z-axis. The angle between the normal and ray is $\theta_1 + \phi$, where $\sin\phi = h_b/R$. The normal of the ray at the second surface is centred at $z = -R + t$. Now the issue is to find relations for h_b and z_b so a projection of the rays propagating through the lens can be plotted. Similarly,

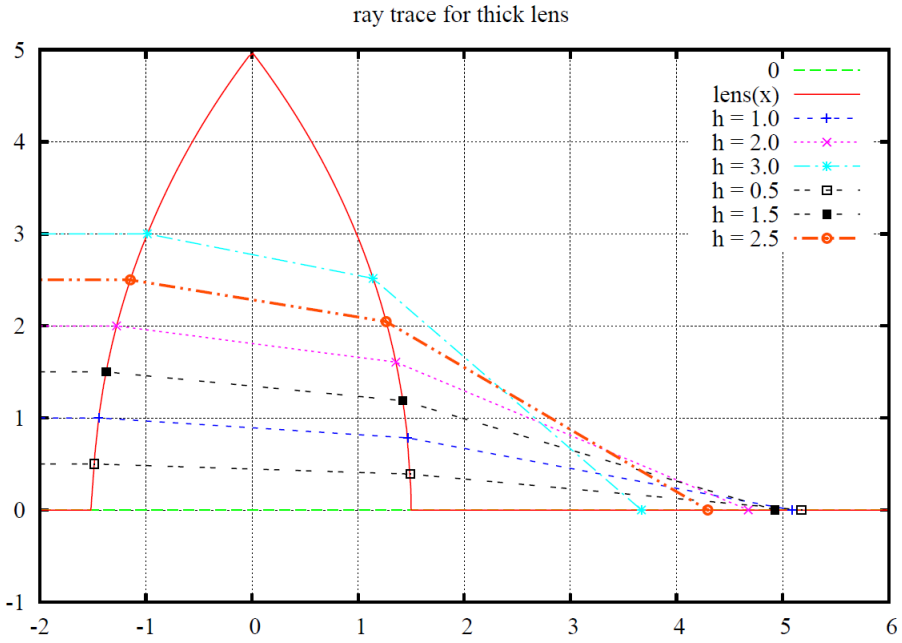

Figure 2.4: Six rays are shown for various heights of h for only upper half of the lens; the lens is symmetric about the z-axis. Refractive index of $n = 1.5$ and thickness $t = 1.5$. Each surface has a radius of $R = 9$ units.

$$\begin{aligned} h_b^2 + (z_b + R - t)^2 &= R^2 \\ h_b^2 + (z_b - t)^2 + 2R(z_b - t) &= 0 \\ (z_b - t) = -R + \sqrt{R^2 - h_b^2} &\approx -\frac{h_b^2}{2R} \end{aligned} \tag{2.36}$$

Another relation for is needed in terms of z_b and h_b in order to produce useful results. If the ray would not pass through the second surface then the ray refracted only by the first surface, at z_a, would cross the axis at point S, where $\tan\theta_1 = h/(S - z_a)$. It is equivalent to say then that $\tan\theta_1 = h_b/(S - z_b)$ also. From here it follows that,

$$\begin{aligned} S &= z_a + \frac{h}{\tan\theta_1} \\ &= z_b + \frac{h_b}{\tan\theta_1}. \end{aligned}$$

Rearranging one obtains,

$$\begin{aligned} h_b &= (S - z_b)\tan\theta_1 \\ h_b^2 &= (S^2 - 2z_bS + z_b^2)\tan^2\theta_1. \end{aligned} \tag{2.37}$$

Substituting Eq. (2.36) into the previous equation yields a quadratic equation for z_b

$$(z_b - S)^2 \tan^2\theta_1 + (z_b + R - t)^2 - R^2 = 0,$$

or

$$Az_b^2 + 2Bz_b + C = 0,$$

where, $A = \sec^2\theta_1$, $B = R - t - S\tan^2\theta_1$, and $C = S^2\tan^2\theta_1 + t^2 - 2Rt$. Solving for z_b yields,

$$z_b = \cos^2\theta_1\left(-B + \sqrt{B^2 - AC}\right). \tag{2.38}$$

Knowing expressions for z_b and h_b a value for ϕ can be found, as $\sin\phi = h_b/R$, and therefore the angle of incidence impinging onto the second surface $\theta_1 + \phi$. By Snell's law the angle of the ray leaving the second surface of the lens is

$$\sin(\theta_2) = n\sin(\theta_1 - \phi).$$

From point z_b the ray is inclined by ϕ, relative to the horizontal, so then the exit rays angle will be $\theta_2 - \phi$. The ray will cross the z-axis at point,

$$z_f = z_b + \frac{h_b}{\tan(\theta_2 - \phi)}.$$

Rays are plotted for several values of h in Fig. 2.4. One can see the rays crossing paths, it is at these points where the interference can lead to a maximum or minimum intensity. Along the caustic adjacent rays are tangential and interfere constructively. There are many points inside the caustic where three rays interfere to give zero intensity. The overall behaviour is known as a diffraction catastrophe.

Chapter 3

Analysis of the Pearcey function

T.Pearcey was the first to do serious calculations of the field amplitude of a spherical lens in the neighbourhood of the cusp, now called the Pearcey function $P(x, y)$. He used the Cambridge "differential analyser", an electro-mechanical machine built by the Metropolitan-Vickers Engineering for Dr Hartree. He first computed $P(x, 0)$ along the real axis using the Watson-Hardy result in terms of Bessel functions of order $\pm 1/4$. Then he solved for $P(x, y)$ at y, by solving a differential equation involving $\partial P/\partial y$. Results were reported graphically as contour plots of modulus and phase for $P(x, y)$.

Pearcey's integral, $P(x, y)$, has numerous nodes and can be analysed via various numerical methods. Authors Stamnes and Spjelkavik [1] Kaminsky and Paris [8] investigated asymptotic approximations of the Pearcey integral in different regions inside the caustic and obtained a high degree of accuracy in finding nodal positions. In this section I will outline the various approximations and their regions of use, but more specifically using this knowledge the region close to the caustic and the lowest order approximation are discussed more closely.

3.1 Approximate solutions to the Pearcey function

T. Pearcey investigated a two parameter integral of a cylindrical electromagnetic wave in 1946 [2], which is now known as the Pearcey integral. Using this integral the field structure near the cusp was numerically studied. Since then the Pearcey integral has been used to study cusps and develop asymptotic approximations of the field structure.

Pearcey's integral takes the form,

$$P(x, y) = \int_{-\infty}^{\infty} e^{i(t^4+t^2x+ty)} dt, \tag{3.1}$$

where the phase function represents the cusp catastrophe. The phase is denoted by

$$h(t) = t^4 + t^2x + ty \tag{3.2}$$

and if

$$h'(t) = 4t^3 + 2tx + y > 0 \tag{3.3}$$

then the real root is given by

$$t_1 = u + v \tag{3.4}$$

where

$$u^3 = -\frac{y}{2} - \sqrt{\frac{y^2}{4} + \frac{x^3}{27}} \tag{3.5}$$

and

$$v^3 = -\frac{y}{2} + \sqrt{\frac{y^2}{4} + \frac{x^3}{27}} \tag{3.6}$$

The two complex roots are complex conjugates and are given by multiplying the root given by Eq. (3.4) by $(-\frac{1}{2} \pm i\frac{\sqrt{3}}{2})$, i.e.,

$$t_{2,3} = (u + v)(-\frac{1}{2} \pm i\frac{\sqrt{3}}{2}) \tag{3.7}$$

If derivative of the phase is negative,

$$h'(t) = 4t^3 + 2tx + y < 0 \tag{3.8}$$

then Eq. (3.4) has three real roots

$$t_1 = 2(-\frac{1}{6}x)^{1/2}\cos(\frac{1}{3}\phi) \tag{3.9}$$

and

$$t_\pm = -2(-\frac{1}{6}x)^{1/2}\cos(1/3(\phi \pm \pi)) \tag{3.10}$$

$$t_2 = t_+, \quad t_3 = t_-$$

where

$$\cos(\theta) = \frac{1}{8}y(-\frac{1}{6}x)^{-3/2} \tag{3.11}$$

From the discussion associated with Eq. (2.16) one can see when $h'(t) < 0$ that as x and y approach zero from the negative side, i.e., $\theta \to 0$, that t_2 and t_3 real roots will coalesce. Also if $h'(t) > 0$ and $\theta \to 0$ from the positive x side of the caustic then the two imaginary stationary points will coalesce into one real stationary point. This means that inside the caustic defined by

$$8x^3 + 27y^2 = 0 \tag{3.12}$$

there are three stationary points, on the caustic itself there are two distinct stationary points and outside only one real stationary point.

3.2 Taylor Series method for small values of R

To compute values for of the Pearcey function for small values of $x^2 + y^2 \equiv R^2 < 16$ one can use the Taylor series. To begin,

$$P(x,y) = \int_{-\infty}^{\infty} e^{i(t^4+xt^2)} \cos(yt)\ dt. \tag{3.13}$$

The power series is obtained by expanding the integrand in powers of x, y and keeping the e^{it^4} term as is. (Odd powers y vanish after integrating over t as $P(x,y)$ is symmetric about the y-axis), everything depends upon interpreting the integrals as gamma functions:

$$\Gamma(z+1) = \int_0^{\infty} t^z e^{-t} dt \tag{3.14}$$

We start with:

$$P(x,y) = \sum_{n=0}^{\infty}\sum_{m=0}^{\infty} \frac{(iy^2)^n (ix)^m i^n}{(2n)!m!} \times \int_{-\infty}^{\infty} t^{2(n+m)} e^{it^4} dt. \tag{3.15}$$

The factors involving t cancel each other and using $i^{8n} = i^{8m} = i^4 = 1$ where n, m are integers. After considerable work one arrives at,

$$P(x,y) = \frac{1}{2}\sum_{n=0}^{\infty}\sum_{m=0}^{\infty} \frac{y^{2n} x^m i^{(6m+10n+1)/4}}{(2n)!m!} \Gamma\left[\frac{1}{4}(2m+2n+1)\right] \tag{3.16}$$

When $x = 0$ the index n is sufficient and using even and odd values of n, i.e., $n = 2k, (2k+1)$, the equation above becomes,

$$P(0,y) = \frac{1}{2}\left[\sum_k \frac{y^{4k} i^{(20k+1)/4}}{(4k!)} \Gamma(k+1/4) + \sum_k \frac{y^{4k+2} i^{(20k+11)/4}}{(4k+2)!} \Gamma(k+3/4)\right]. \tag{3.17}$$

This can be simplified as $i^{1/4} = e^{i\pi/8}$ and $i^{11/4} = -ie^{-i\pi/8}$

$$2P(0,y) = e^{i\pi/8} \sum_k \frac{y^{4k} i^k}{(4k)!} \Gamma(k+1/4) - ie^{-i\pi/8} \sum_k \frac{y^{4k+2} i^k}{(4k+2)!} \Gamma(k+3/4). \tag{3.18}$$

Write $2P(0,y) = \sum_k$ so as to make clear of the expansion over k. The $k = 0$ term,

$$S_0 = e^{i\pi/8}\Gamma\left(\frac{1}{4}\right) - ie^{-i\pi/8}\frac{y^2}{2!}\Gamma\left(\frac{3}{4}\right). \tag{3.19}$$

The real and imaginary parts of $P(0,y)$ can be combined to give the amplitude and phase. This can be written in a more general form,

$$2P(0,y) = e^{i\pi/8}\left[S_{0r} + iS_{1i}\right] + e^{-i\pi/8}\left[S_{3i} - iS_{2r}\right] \tag{3.20}$$

where,

$$\begin{aligned}
S_{0r} &= \Gamma\left(\frac{1}{4}\right) - \frac{y^8}{8!}\Gamma\left(\frac{9}{4}\right) + \frac{y^{16}}{16!}\Gamma\left(\frac{17}{4}\right) - \dots \\
S_{2r} &= \frac{y^2}{2!}\Gamma\left(\frac{3}{4}\right) - \frac{y^{10}}{10!}\Gamma\left(\frac{11}{4}\right) + \frac{y^{18}}{18!}\Gamma\left(\frac{19}{4}\right) - \dots \\
S_{1i} &= \frac{y^4}{4!}\Gamma\left(\frac{5}{4}\right) - \frac{y^{12}}{12!}\Gamma\left(\frac{13}{4}\right) + \frac{y^{20}}{20!}\Gamma\left(\frac{21}{4}\right) - \dots \\
S_{3i} &= \frac{y^6}{6!}\Gamma\left(\frac{7}{4}\right) - \frac{y^{14}}{14!}\Gamma\left(\frac{15}{4}\right) + \frac{y^{22}}{22!}\Gamma\left(\frac{23}{4}\right) - \dots
\end{aligned} \tag{3.21}$$

The above sums combine to give,

$$\begin{aligned}
2\Re P &= \cos(\pi/8)\left[S_{0r} + S_{3i}\right] - \sin(\pi/8)\left[S_{1i} + S_{2r}\right] \\
2\Im P &= \sin(\pi/8)\left[S_{0r} - S_{3i}\right] - \cos(\pi/8)\left[S_{1i} - S_{2r}\right]
\end{aligned} \tag{3.22}$$

Only S_{0r} is non-zero at the origin, so at $P(0,0)$ the phase is equal to $\pi/8$, with a magnitude of $\frac{1}{2}\Gamma\left(\frac{1}{4}\right)$. A similar operation is done along the x-axis with $y = 0$ but instead of summing over k, one sums only with index m. Separating into even values and odd values of m, $m = 2j, (2j+1)$ yields,

$$2P(x,0) = \sum_j x^{2j}\frac{i^{(12j+1)/4}}{(2j)!}\Gamma\left(j + \frac{1}{4}\right) + \sum_j x^{2j+1}\frac{i^{(12j+7)/4}}{(2j+1)!}\Gamma\left(j + \frac{3}{4}\right). \tag{3.23}$$

Using $i^4 = 1$, $i^{1/4} = e^{i\pi/8}$ and $i^{7/4} = i^2 e^{-i\pi/8}$, one can write

$$\begin{aligned}
2P(x,0) &= e^{i\pi/8}\sum_j x^{2j}\frac{(-i)^j}{(2j)!}\Gamma\left[j + \frac{1}{4}\right] - e^{-i\pi/8}\sum_j x^{2j+1}\frac{(-i)^j}{(2j+1)!}\Gamma\left[j + \frac{3}{4}\right] \\
&= e^{i\pi/8}\left[S_{er} - iS_{ei}\right] - e^{-i\pi/8}\left[S_{or} - iS_{oi}\right].
\end{aligned} \tag{3.24}$$

Here the e, o subscripts denote the powers of x to be either odd or even. Assuming x is positive,

$$
\begin{aligned}
S_{er} &= \Gamma\left(\frac{1}{4}\right) - \frac{x^4}{4!}\Gamma\left(\frac{9}{4}\right) + \frac{x^8}{8!}\Gamma\left(\frac{17}{4}\right) - \dots \\
S_{or} &= \frac{x}{1!}\Gamma\left(\frac{3}{4}\right) - \frac{x^5}{5!}\Gamma\left(\frac{11}{4}\right) + \frac{x^9}{9!}\Gamma\left(\frac{19}{4}\right) \dots \\
S_{ei} &= \frac{x^2}{2!}\Gamma\left(\frac{5}{4}\right) - \frac{x^6}{6!}\Gamma\left(\frac{13}{4}\right) + \frac{x^{10}}{10!}\Gamma\left(\frac{21}{4}\right) \dots \\
S_{oi} &= \frac{x^3}{3!}\Gamma\left(\frac{7}{4}\right) - \frac{x^7}{7!}\Gamma\left(\frac{15}{4}\right) + \frac{x^{11}}{11!}\Gamma\left(\frac{23}{4}\right) \dots
\end{aligned} \tag{3.25}
$$

Combining these sums yields,

$$
\begin{aligned}
2\Re P &= \cos\left(\frac{\pi}{8}\right)[S_{er} - S_{or}] + \sin\left(\frac{\pi}{8}\right)[S_{ei} + S_{oi}] \\
2\Im P &= \sin\left(\frac{\pi}{8}\right)[S_{er} + S_{or}] - \cos\left(\frac{\pi}{8}\right)[S_{ei} - S_{oi}] .
\end{aligned} \tag{3.26}
$$

When $x \to -x$, the amplitudes S_{er} and S_{ei} stay the same but S_{or} and S_{oi} change sign. This makes the $-x$ landscape very different from the positive landscape. For the opposite sign of x one has,

$$
\begin{aligned}
2\Re P &= \cos\left(\frac{\pi}{8}\right)[S_{er} + S_{or}] + \sin\left(\frac{\pi}{8}\right)[S_{ei} - S_{oi}] \\
2\Im P &= \sin\left(\frac{\pi}{8}\right)[S_{er} - S_{or}] - \cos\left(\frac{\pi}{8}\right)[S_{ei} + S_{oi}] .
\end{aligned} \tag{3.27}
$$

According to Stamnes [1] these equations for the values of the Pearcey function give good results up to $x \approx 4$ with $y = 0$, after which requires it too many terms to achieve convergence. We did not succeed in getting reasonable results.

3.3 Method of stationary phase

In order to deduce values for the asymptotic behaviour of $P(x, y)$, at large x one can use the method of stationary phase. The Pearcey function in the negative x axis is,

$$
P(-x, y) = \int_{-\infty}^{\infty} e^{i(t^4 - xt^2 + yt)} dt. \tag{3.28}
$$

Let $t = \sqrt{x}u$,

$$
\begin{aligned}
P(-x, y) &= \sqrt{x} \int_{-\infty}^{\infty} e^{ix^2(u^4 - u^2 + yx^{-3/2}u)} du \\
&= \sqrt{x} \int_{-\infty}^{\infty} e^{ix^2\psi(u)} du
\end{aligned} \tag{3.29}
$$

In general to calculate along paths of steepest descent one considers the integral in the form

$$I(\lambda) = \int_C g(z) e^{\lambda w(z)} dz. \tag{3.30}$$

The contour of integration is chosen so that the real part of $w(z)$ approaches minus infinity at both limits and the integrand vanishes. If λ is a large positive number the value of the integrand is large when real $w(z)$ is large and small when real $w(z)$ is small or negative. The main contribution of the integrand will come from the region where the real part of $w(z)$ has a maximum value. Away from positive maximum the integrand will become negligible. Writing,

$$w(z) = u(x, y) + iv(x, y). \tag{3.31}$$

Separating into real and imaginary parts, the integral is then,

$$I(\lambda) = \int_C g(z) e^{\lambda u(x,y)} e^{i\lambda v(x,y)} dz. \tag{3.32}$$

It is important that the maximum value of $u(x, y)$ is maximum only along a contour. In the finite plane neither the real nor imaginary parts can possess an absolute maximum value as u and v both satisfy Laplace's equation,

$$\begin{aligned} \frac{\partial^2 u}{\partial x^2} + \frac{\partial^2 u}{\partial y^2} &= 0 \\ \frac{\partial^2 v}{\partial x^2} + \frac{\partial^2 v}{\partial y^2} &= 0. \end{aligned} \tag{3.33}$$

If u or v curve downwards along x, then they want to curve up along y and vice versa. The contour must be chosen so that $u(x, y)$ has a maximum at the saddle point and the contour must pass through the saddle in such a way that the imaginary part $v(x, y)$ is constant along the path. One can then say,

$$I(\lambda) \approx e^{i\lambda v_0} \int_C g(z) e^{\lambda u(x,y)} dz. \tag{3.34}$$

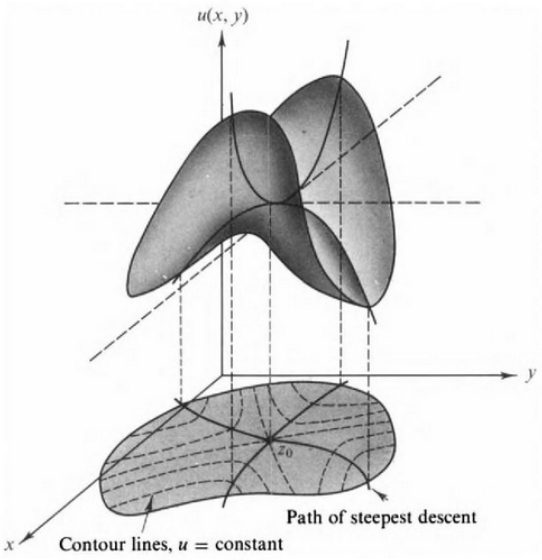

Figure 3.1: Path of steepest descent

Curves corresponding to u = constant and v = constant form an orthogonal system, in other words, a curve $v = c_i$ is everywhere tangential to ∇u. Therefore the curve v = constant is the curve that gives the line of steepest descents from the saddle point. Fig. 3.1 comes from Arfken. [13] page 430. One can see the function has a maximum along the direction of steepest descent. If the contour is deformed in such a way that it passes through the saddle point in the direction of steepest descent, the large values of λ ensure that essential contributions for the integrand come from a small region near the saddle point as the exponent quickly decreases. The detailed shape of the curve of steepest descent far from the saddle point is unimportant. To evaluate the Pearcey function one makes one makes the following substitutions in Eq. (3.30),

$$\begin{aligned} z &= u \\ \lambda &= x^2 \\ i\psi(u) &= w(z) \\ \sqrt{x} &= g(z) = const. \end{aligned} \tag{3.35}$$

Setting $\gamma = yx^{-3/2}$ for simplicity of notation the phase $w(z)$ becomes,

$$w(z) = i(z^4 - z^2 + \gamma z). \tag{3.36}$$

In order to find the angle that the path makes between the real axis and the path one follows the recipe given in Bleistein and Handelman [14]. Take the second derivative

with respect to z and set to $z = u_1$, i.e the first stationary point,

$$\begin{aligned} \frac{d^2w}{dz^2} &= i(12z^2 - 2) = 2i(6z^2 - 1) \\ (\frac{d^2w}{dz^2})_{z=u_1} &= 2i(6u_1^2 - 1) = i2d_1^2 = 2d_1^2 e^{i\pi/2}. \end{aligned} \tag{3.37}$$

From Table 7.1 in Bleistein one obtains the angle of the path of steepest descents to the real axis as

$$\theta_p = -\frac{\alpha}{n} + (2p+1)\frac{\pi}{n}, \tag{3.38}$$

where $p = 0, 1, 2..n-1$. For u_1 $n = 2$ and $\alpha = \pi/2$. In this case the angles $\theta_0 = \pi/4$, $\theta_1 = \pi + \pi/4, \ldots$ for the slope going through the node u_1. For the second node u_2 the phase is written as

$$w(z) = i(z^4 - z^2 + \gamma z) \tag{3.39}$$

and the second derivatives lead to

$$\begin{aligned} \frac{d^2w}{dz^2} &= i(12z^2 - 2) = -2i(1 - 6z^2) \\ (\frac{d^2w}{dz^2})_{z=u_2} &= -2i(1 - 6u_2^2) = -i2d_2^2 = 2d_2^2 e^{-i\pi/2}. \end{aligned} \tag{3.40}$$

Eq. (3.38) gives angles $\theta_0 = 3\pi/4,\ \theta_1 = 3\pi/4 + \pi \ldots$ as $n = 2$ and $\alpha = -\pi/2$. Root u_3 behaves the same as the first root u_1.

According to Bleistein [14] the steepest descent paths are curves where the imaginary part of the phase is constant. One writes,

$$\begin{aligned} w(z) &= u(x,y) + iv(x,y), \\ u(x,y) &= -4x^3y + 4xy^3 + 2xy - \gamma y, \\ v(x,y) &= x^4 - 6x^2y^2 + y^4 - x^2 + y^2 + \gamma x. \end{aligned} \tag{3.41}$$

Therefore if we want to find the relation between x and y which contains the phase then we must equate $v(x,y)$ to the value at the stationary point. Then the imaginary component is also equal to the form of the phase which contains information about the roots,

$$x^4 - 6x^2y^2 + y^4 - x^2 + y^2 + \gamma x = u_i^4 - u_i^2 + \gamma u_i. \tag{3.42}$$

This can be rearranged in the form of a quadratic in y^2,

$$y^4 + (1+6x^2)y^2 + (x^4 - x^2 + \gamma x - (u_i^4 - u_i^2 + \gamma u_i)) = 0. \tag{3.43}$$

whose solution is,

$$\begin{aligned} y_i^2(x) &= \frac{1}{2}(-1 + 6x^2 \pm \sqrt{\Delta_i}) \\ \Delta_i &= (1-6x^2)^2 - 4(x^4 - x^2 + \gamma x - (u_i^4 - u_i^2 + \gamma u_i)). \end{aligned} \tag{3.44}$$

When the discriminant Δ_i is positive then one has two real values of y^2. Δ_i specifies x, y on the path of stationary phase. Paths of constant phase are those which have fewest cancellations between the plus and minus values, so better numerical accuracy can be obtained. The next step is to investigate the paths via numerical integration to see the variation of the root $u(x, y_i)$ along the contour.

$$P(x_0, y_0) = \sqrt{x_0} \sum_{u_i} e^{i x_0^2 v_i} \int_{-\infty}^{\infty} e^{x_0^2 u(x, y_i)} ds \tag{3.45}$$

where,

$$\begin{aligned} ds_i &= \sqrt{1 + (\frac{dy}{dx})^2}\ e^{i\xi_i}\ dx \\ (\frac{dy}{dx})_i &= -\frac{\partial v/\partial x}{\partial v/\partial y} = \frac{-4x^3 + 12xy_i^2 + 2x - \gamma}{-12x^2 y_i + 4y_i^3 + 2y_i} \\ \xi_i &= \arctan(\frac{dy}{dx})_i + \Lambda_i\,. \end{aligned} \tag{3.46}$$

We use $\int dx = \int \left(\frac{dx}{ds}\right) ds$ where ds is step size along the path. There is a problem in that path Γ_1 has a vertical section when $x > u_1$ and path Γ_3 similarly when $x < u_3$. On these sections one uses $\int dy = \int \left(\frac{dy}{ds}\right) ds$ instead. The Taylor expansion for $y'(x)$ is performed,

$$y'(x) \approx 1 + \frac{8u_i}{1-6u_i^2}(x - u_i) + 2\frac{(3 + 47u_i^2)}{(1-6u_i^2)^2}(x - u_i^2)^2 \tag{3.47}$$

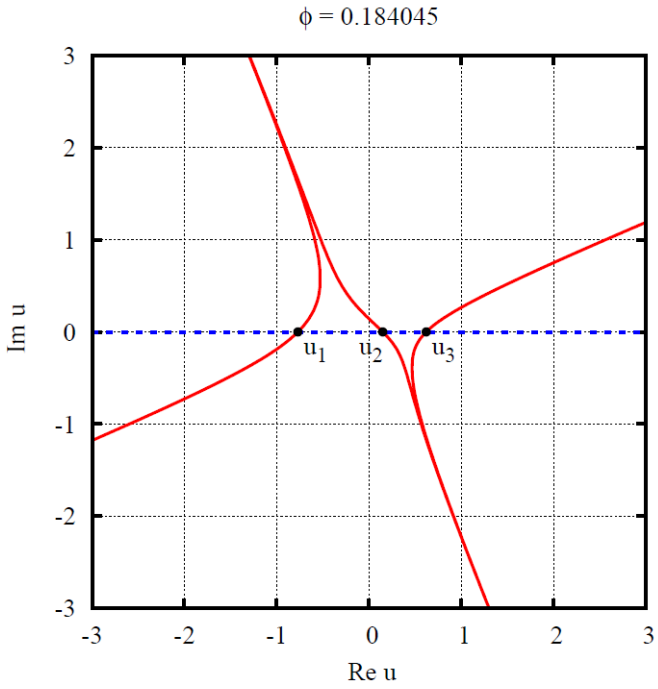

Figure 3.2: Paths of constant phase in complex u plane. Contours are inclined asymptotically at an of angle $\pi/8$ relative to the real/imaginary axes. The three branches pass through the three stationary points on the real axis. The contours pass through the stationary points u_1 and u_3 at an angle of $\pi/4$, whilst u_2 is traversed at an angle of $-\pi/4$.

Looking at the contour lines of $|P|$ in Fig. A.1 in the Appendix, taken from [1], one sees that the nodes appear mostly in vertical pairs. The lowest contour lines $|P| = 0.2$ are rather egg-shaped, long vertically and shorter horizontally. In plotting $|P|$ on a small circle surrounding the node, $-x = 11.4774412231$, $y = 1.639203731$, the values at angle zero will be will be higher than the values at points vertical. Indeed that is what is seen in Figs. 3.3 and 3.4. They show that the calculated values must be accurate to order 10^{-8}, or else the curves would be erratic, as in Fig. 3.5.

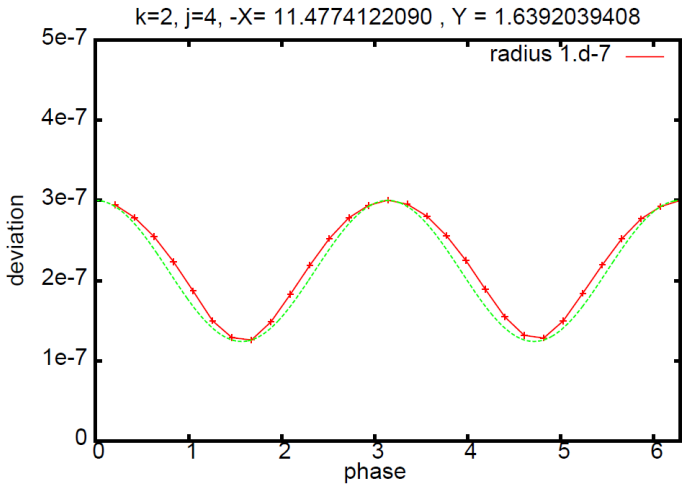

Figure 3.3: $|P(-x, y)|$ on a circle of radius 10^{-7} around a node with a cosine curve for comparison.

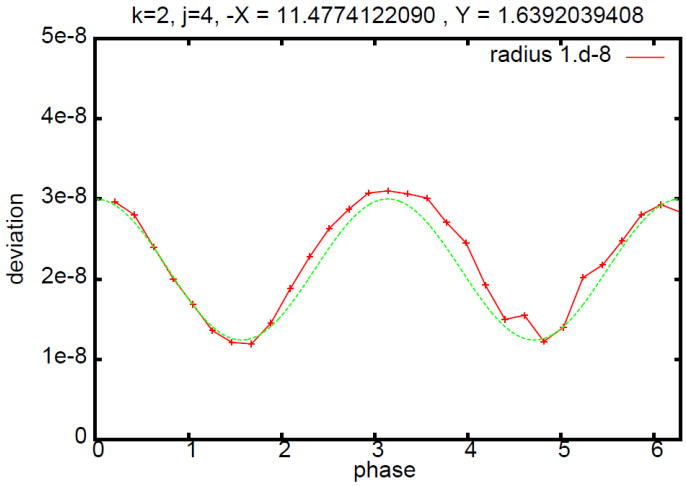

Figure 3.4: $|P(-x, y)|$ on a circle of radius 10^{-8}.

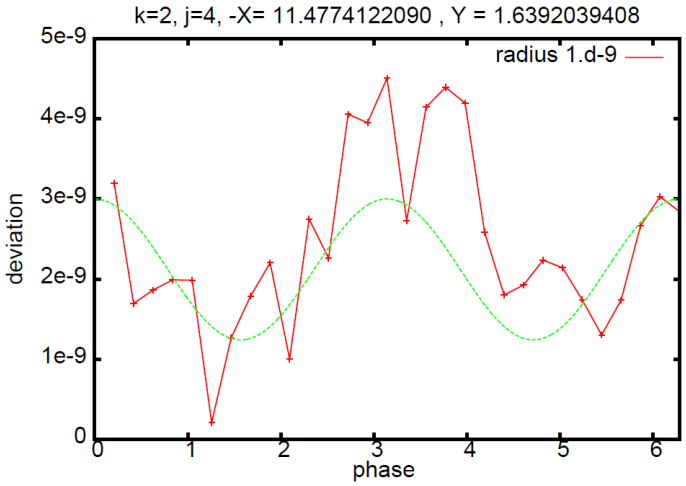

Figure 3.5: $|P(-x, y)|$ on a circle of radius 10^{-9}.

Further, suppose that the nodal position is inaccurate. If the node were thought to be a little to the right, the value of $|P|$ would be too high at angle zero, and too low at angle π. Rather than a $\cos\theta$ curve one would see a $\cos(2\theta)$ curve with a single minimum at π. Since we do not see any such behaviour, we deduce that the nodal point position is also accurate to order 10^{-8}.

Fig. 3.6 is for another node around which we plot $|P|$ on a square grid of points spaced 5×10^{-9} apart. The surface is reasonably smooth with the minimum value of order 2×10^{-8} located near point $(5, 7)$. Contour lines of $|P|$ drawn on the base plane show elliptical shape.

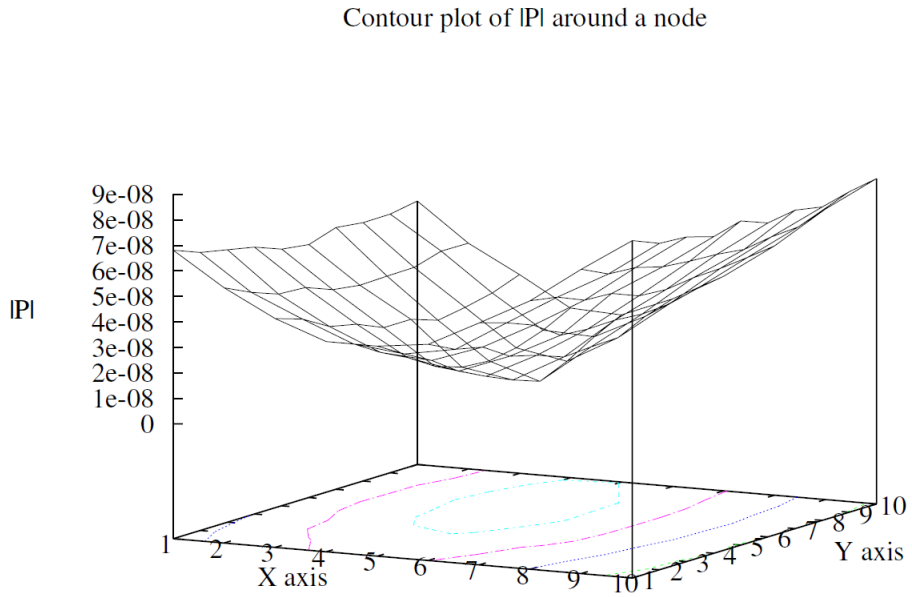

Figure 3.6: Values of $|P|$ on a square grid around an approximate node. Contour lines are projected onto the zero plane. One unit of x and y corresponds to 5×10^{-9}.

3.4 Systematic method to find the nodal points

Kaminsky and Paris [8] developed asymptotic approximations for finding nodal positions of the Pearcey function. The work involved using method of steepest descents to evaluate the integral as long as the x^2 term in the exponent is large enough to justify this. The phase function is written in this form,

$$\psi(u) = u^4 - u^2 + yx^{-3/2}u. \tag{3.48}$$

The stationary points are located where the phase, $\psi'(u) = 0$, vanishes. This is a cubic equation,

$$\frac{1}{4}\psi'(u) = u^3 - \frac{1}{2}u + \frac{1}{4}yx^{-3/2} \tag{3.49}$$

$$\frac{1}{4}\psi'(u) = (u - u_1)(u - u_2)(u - u_3). \tag{3.50}$$

Equation (3.50) is satisfied if

$$\begin{aligned} \sum u_i &= 0 \\ \sum u_i u_j &= -\frac{1}{2} \\ u_1 u_2 u_3 &= -yx^{-3/2}/4. \end{aligned} \tag{3.51}$$

At a node of $\psi'(u)$ Eqs. (3.48) and (3.49) can be combined to express.

$$\psi(u_i) = -\frac{1}{2}u_i^2 + \frac{3}{4}yx^{-3/2}u_i \tag{3.52}$$

Next Kaminsky and Paris state that the the solutions the three roots of the cubic Eq. (3.49) can be parametrised as such

$$u_1 = -\sqrt{\frac{2}{3}}\sin(\frac{\pi}{3} + \theta)$$

$$u_2 = \sqrt{\frac{2}{3}}\sin(\theta)$$

$$u_3 = \sqrt{\frac{2}{3}}\sin(\frac{\pi}{3} - \theta)$$

where

$$\sin(3\theta) = \frac{3\sqrt{3}}{2\sqrt{2}}\frac{y}{x^{3/2}}. \tag{3.53}$$

The caustic corresponds to the case when $\theta = \pi/6$ which means that the roots u_2 and u_3 coalesce. To find the values of the nodes inside the caustic the method of steepest descents involves three path integrals. The path integrals must pass through each stationary point and must be rotated from the lying on the real axis. The left most contour Γ_1 is rotated and starts at a point $A = \infty e^{i9\pi/8}$ and ends at $B = \infty e^{i5\pi/8}$ passing through u_1. In order to pass through the stationary points the contours are stretched. Contour Γ_2 starts at $B = \infty e^{i5\pi/8}$ and and ends at $C = \infty e^{-i3\pi/8}$ passing through u_2. Contour Γ_3 starts at $C = \infty e^{-i3\pi/8}$ passes u_3 ends at $D = \infty e^{i\pi/8}$. The total contour is a sum of three branches Γ_j as shown in Fig. 3.2, with $\Gamma_1 = A \to B$, $\Gamma_2 = B \to C$ and $\Gamma_3 = C \to D$ with each contour Γ_j passing through point u_j. This can be represented in the form,

$$P(-x, y) = \sqrt{x}\sum_{j=1}^{3}\int_{\Gamma_j} e^{ix^2\psi(u)}du. \tag{3.54}$$

To evaluate in Eq. (3.54) the function in the exponent, the simplest approximation is to replace the exponent by a negative valued quadratic function of u along the path

of integration. To do this the ix^2 must go like $-x^2$. Since $\psi(u) \approx \psi(u_j) + d_j^2(u-u_j)^2$, then $(u-u_j)^2 \approx i$ for the approximation to be carried out along the real axis. That is $(u-u_j) = \sqrt{i}v_j$ on the path of integration, close to u_j. Since a polynomial of degree N remains as such, near u_j the function in the exponent can be written

$$\psi(u) = \psi(u_j) + \frac{1}{2}\psi''(u_j)(u-u_j)^2 + \frac{1}{3!}\psi'''(u_j)(u-u_j)^3 + \frac{1}{4!}\psi''''(u_j)(u-u_j)^4 \quad (3.55)$$

$$\psi(u) = \psi(u_j) + [6u_j^2 - 1](u-u_j)^2 + 4(u-u_j)^3 + (u-u_j)^4 \quad (3.56)$$

which reduces when we keep only the quadratic bit, to

$$\psi(u) \approx \psi(u_j) + (-)^{j+1}d_j^2 v^2, \quad (3.57)$$

where,

$$v = (u-u_j)[1 + \frac{4u_j(u-u_j)}{d_j^2} + \frac{(u-u_j)^2}{d_j^2}]^{1/2} \quad (3.58)$$

$$(d_1)^2 = 6u_1^2 - 1 = 1 + 2\cos 2\epsilon \quad (3.59)$$

$$(d_2)^2 = 1 - 6u_2^2 = 2\cos 2\theta - 1 \quad (3.60)$$

$$(d_3)^2 = 6u_3^2 - 1 = 1 + 2\cos 2\theta, \quad (3.61)$$

where $\epsilon = \pi/6 - \theta$ and $(u-u_j)$ is a complex value. There terms in the square brackets for v is only needed for going beyond the lowest order of steepest descents, which will not be done here. Instead v will be set as $v^2 = \pm i(u-u_j)^2$. If one were wanting to go beyond the leading order expansion the Eq. (3.58) can be rearranged to yield an expression for $u - u_j$ in powers of v such as,

$$u - u_j = v + \sum_{k=2} b_{k,j} v^k. \quad (3.62)$$

Now each contour integral is given by

$$\int_{\Gamma_j} e^{ix^2\psi(u)}du = \frac{e^{(ix^2\psi(u_j) - i\pi/4(-)^j)}}{xd_j} \times \sum_{k=0}(2k+1)b_{2k+1,j}\frac{\Gamma(k+1/2(-)^{j+1}i^k}{x^{2k}d_j^{2k}}, \quad (3.63)$$

which defines $a_{2r,j}$. This simplifies to

$$P(-x,y) \approx \sqrt{\frac{\pi}{x}}\sum_{j=1}^{3}\frac{e^{(ix^2\psi(u_j) - i\pi/4(-)^j)}}{d_j} \times \sum_{r=0}\frac{i^r a_{2r,j}}{x^{2r}}. \quad (3.64)$$

So then by this approximation each stationary point contributes an asymptotic estimate proportional to

$$P_j(-x,y) = \sqrt{\frac{\pi}{x}}\frac{e^{ix^2\psi(u_j)}}{d_j}\left[1+\sum_{r=1}\frac{i^r a_{2r,j}}{x^{2r}}\right] \equiv \sqrt{\frac{\pi}{x}}\frac{e^{iA_j}}{D_j} \tag{3.65}$$

where $A_j = x^2\psi(u_j)+\sigma_j$ and $D_j = d_j/(1+s_j)$

$$\sigma_j \equiv \arg\left[1+\sum_{r=1}\frac{i^r a_{2r,j}}{x^{2r}}\right] \approx \frac{a_{2,j}}{x^2}+\mathcal{O}(x^{-4}) \tag{3.66}$$

$$1+s_j \equiv \mathrm{mod}\left|1+\sum_{r=1}\frac{i^r a_{2r,j}}{x^{2r}}\right| \tag{3.67}$$

and the leading coefficient is

$$a_{2,j} = \frac{1}{4d_j^4}\left[7+\frac{10}{(-)^{j+1}d_j^2}\right]. \tag{3.68}$$

Kaminsky and Paris initially ignored these higher order corrections, eventually they included $1/x^2$ corrections. However, in this thesis we do not consider this embellishment.

3.5 Zeroth Order

For zeroth order the σ_j term is ignored and $D_j = d_j$ from Eq. (3.65). So then the approximation of the Pearcey function is rewritten as

$$P(-x,y) \approx \sqrt{\frac{\pi}{x}}\left[\frac{e^{iA_2+i\pi/4}}{d_1}+\frac{e^{iA_2-i\pi/4}}{d_2}+\frac{e^{iA_3+i\pi/4}}{d_3}\right], \tag{3.69}$$

Setting Eq. (3.69) to zero and separating into real and imaginary components leads to two equations

$$\frac{\cos A_1}{d_1}+\frac{\sin A_2}{d_2}+\frac{\cos A_3}{d_3} = 0 \tag{3.70}$$

$$\frac{\sin A_1}{d_1}-\frac{\cos A_2}{d_2}+\frac{\sin A_3}{d_3} = 0. \tag{3.71}$$

Using Eqs. (3.71) and (3.70) one can modify these equations by taking the middle term from each equation and moving them to the right hand side, squaring the equations and adding them together, to yield

$$\frac{1}{d_1} - \frac{1}{d_2} + \frac{1}{d_3} = \frac{2}{d_1 d_3}\cos(A_1 - A_3). \tag{3.72}$$

The result of the left hand side vanishes according to Kaminsky and Paris as if one were to view the equation in terms of u_j, the function is a symmetric function of the u_j. Therefore it is possible to evaluate the left side of the equation in terms of the coefficients $\psi'(u) = 0$. Allowing one to write a simpler result,

$$0 = \cos(A_1 - A_3). \tag{3.73}$$

It follows that $A_3 - A_1 = (k + 1/2)\pi$, for some integer values of k. Going back to the result in Eq. (3.52)

$$\begin{aligned} A_3 - A_1 &= x^2\left[\psi(u_3) - \psi(u_1)\right] \\ &= x^2\left[-\frac{1}{2}\left(u_3^2 - u_1^2\right) + \frac{3}{4}yx^{-3/2}\left(u_3 - u_1\right)\right] \\ &= x^2(u_3 - u_1)\left[-\frac{1}{2}(u_3 + u_1) + \frac{3}{4}yx^{-3/2}\right] \\ &= x^2(u_3 - u_1)\left[\frac{1}{2}u_2 + \frac{3}{4}yx^{-3/2}\right] \geq 0. \end{aligned} \tag{3.74}$$

Now as each factor is positive one can say

$$A_3 = A_1 + (k + \frac{1}{2})\pi \tag{3.75}$$

where k is a positive integer, $k = 1, 2, ...$ This implies that $\cos A_1 = (-)^k \sin A_3$ and $\sin A_1 = -(-)^k \cos A_3$ so then Eqs. (3.70) and (3.71) can be restated as

$$\begin{aligned} \frac{(-)^k \sin A_3}{d_1} + \frac{\cos A_3}{d_3} &= -\frac{\sin A_2}{d_2} \\ \frac{(-)^k \cos A_3}{d_1} - \frac{\sin A_3}{d_3} &= -\frac{\cos A_2}{d_2} \end{aligned} \tag{3.76}$$

To simplify the above, consider a right angled triangle with sides $d_1, d_3, \sqrt{d_1^2 + d_3^2}$. This defines an angle α such that,

$$\tan\alpha = d_1/d_3, \qquad \sin\alpha = \frac{d_1}{\sqrt{d_1^2 + d_3^2}}, \qquad \cos\alpha \frac{d_3}{\sqrt{d_1^2 + d_3^2}}$$

Then Eqs. (3.70) and (3.71) can be rewritten as

$$\begin{aligned}(-)^k \sin A_3 \cos\alpha + \cos A_3 \sin\alpha &= \sin(A_2+\pi)\\ (-)^k \cos A_3 \cos\alpha - \sin A_3 \sin\alpha &= \cos(A_2+\pi).\end{aligned} \tag{3.77}$$

When k is even

$$\begin{aligned}\sin(A_3+\alpha) &= \sin(A_2+\pi)\\ \cos(A_3+\alpha) &= \cos(A_2+\pi)\end{aligned} \tag{3.78}$$

from which it follows that

$$A_2 - A_3 = \alpha + (2j+1)\pi \tag{3.79}$$

for some integer value of j. When k is odd,

$$\begin{aligned}\sin(A_3-\alpha) &= \sin A_2\\ \cos(A_3-\alpha) &= \cos A_2,\end{aligned} \tag{3.80}$$

from which it follows

$$A_3 - A_2 = 2\pi - \alpha + (2j)\pi. \tag{3.81}$$

The difference of $(A_2 - A_3)$ when j is even is $(2j+1)\pi + \alpha$, or j is odd state is $(2j+1)\pi + (\pi - \alpha)$, where $j = 1, 2, 3....$

Eq. (3.53) sets $\lambda = \sin(3\theta)$ which covers all locations inside the caustic where the nodes might be, for $0 < \theta < \pi/6$. So then the next step is to relate this zeroth order approximation to θ and generate values for nodal positions. With

$$\begin{aligned}A_2 - A_3 &= x^2(\psi(u_2) - \psi(u_3))\\ &= \frac{2x^2}{\sqrt{3}} \sin^2\left(\theta - \frac{\pi}{6}\right)\ \cos\left(2\theta + \frac{\pi}{6}\right)\\ &= 2j\pi + \begin{cases}\pi+\alpha, & k \quad \text{even}\\ 2\pi-\alpha, & k \quad \text{odd}\end{cases}\end{aligned} \tag{3.82}$$

Eq. (3.82) allows one to write x^2 in terms of θ, j, α. In a similar way, the difference between $A_3 - A_1$ in terms of θ can be written as

$$\begin{aligned}A_3 - A_1 &= x^2(\psi(u_3) - \psi(u_1))\\ &= \frac{2x^2}{\sqrt{3}} \sin 2\theta \cos^2\theta\end{aligned} \tag{3.83}$$

which can be rewritten as,

$$x^2 = \frac{\sqrt{3}(k+\frac{1}{2})\pi}{2\sin 2\theta \cos^2\theta}. \tag{3.84}$$

Equating the two values we just obtained for x^2 from Eq. (3.84) and Eq. (3.82) leads to Eq. (3.85) where only θ, j, k remain,

$$(k+\frac{1}{2})\pi \frac{\sin^2(\theta-\pi/6)\cos(2\theta+\pi/6)}{2\sin 2\theta\cos^2\theta} = 2j\pi + \begin{cases} \pi+\alpha, & k \quad \text{even} \\ 2\pi-\alpha, & k \quad \text{odd} \end{cases} \tag{3.85}$$

The trigonometric function in Eq. (3.85) can be conveniently be rewritten as,

$$S(\theta) = \frac{\sin^3(\epsilon)\cos(\epsilon)}{\sin(\theta)\cos^3(\theta)}, \tag{3.86}$$

where we define $\epsilon \equiv \pi/6 - \theta$. A numerical solution for θ can be found by solving for θ,

$$S(\theta) = \frac{2j + 3/2 - (-)^k\beta}{k+1/2} \tag{3.87}$$

where k, j are chosen integers and β is the angle to the extreme right of Eq. (3.85).

By solving Eq. (3.87) one finds values for θ for given input of the labels k and j. The routine bisection was used from pages 1184-1185 of [15]. Values for θ are found within $0 < \theta < \pi/6$. Once a value for θ is produced one can obtain approximate positions for the nodes. x, y are generated via Eq. (3.88) and the image below shows the nodal positions inside the caustic with corresponding k, j labels.

$$\begin{aligned} x &= \sqrt{\frac{\sqrt{3}(k+1/2)\pi}{2\sin 2\theta\cos^2\theta}} \\ y &= \left(\frac{2}{3}x\right)^{3/2}\sin 3\theta \end{aligned} \tag{3.88}$$

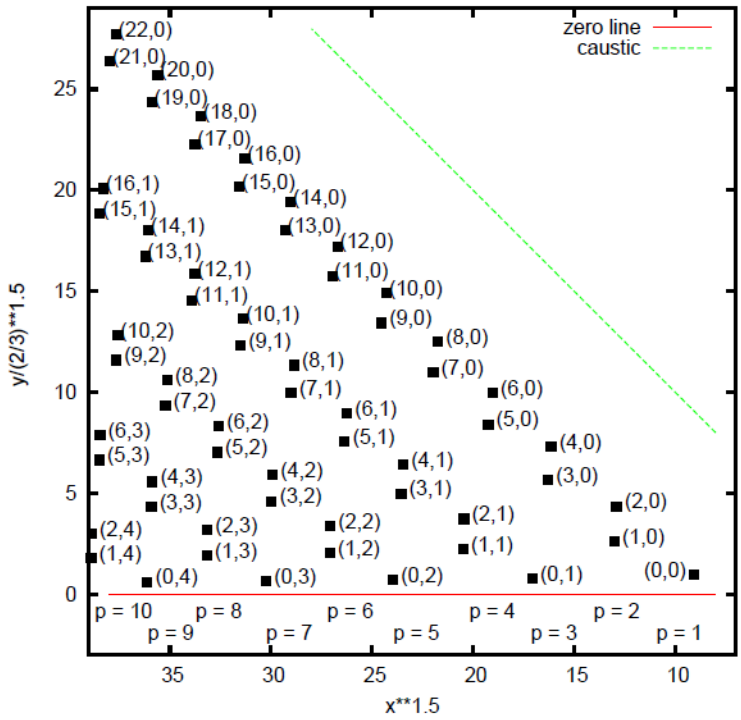

Figure 3.7: Location of the nodes inside the caustic are presented here with (k, j) indexing labels.

When j is fixed and k varies, one generates nodes which are parallel to the caustic. If k is fixed and j varies, nodes are generated which are roughly parallel to the x-axis. The axes have been modified to present the caustic as a straight line. The x-axis is changed to $x^{3/2}$ and y-axis is $y/(2/3)^{3/2}$. Nodes occur in sets of $p = 1, 2, 3 \ldots$ at $x = x_p$. The p label corresponds to the number of nodes in a family. For example the single node of $k = 0, j = 0$ corresponds to $p = 1$. The pair of nodes further left $(1, 0)$ and $(2, 0)$ corresponds to the $p = 2$ family and $p = 3$ corresponds to $(0, 1)$,$(3, 0)$ and $(4, 0)$ etc. It should also be noted here that the caustic is in the $-x$ region but for convenience the minus sign has been omitted. One can also notice that within a p-family, the sum of $k + 4j$ is a constant, or a constant minus one. For example $p = 5$, $k + 4j = 7$ or 8

3.6 Line of nodes outside the caustic

Outside of the caustic there is a line of nodes running more or less parallel to the caustic. The nodes outside have one real root u_1 and two complex conjugate roots $u_2, u_3 = u_2^*$, which have coalesced when $\theta = \pi/6$. The stationary points outside are parametrised as,

$$\begin{aligned} u_1 &= -\frac{2}{\sqrt{6}}\cosh(\theta) \\ u_2 &= \frac{1}{\sqrt{6}}\cosh(\theta) + \frac{i}{\sqrt{2}}\sinh(\theta) = u_3^*. \end{aligned} \tag{3.89}$$

This is consistent with KP's equations for the stationary points inside the caustic. Define $\theta = \pi/6 - \epsilon$.

$$\begin{aligned} u_1 &= -\frac{2}{\sqrt{6}}\cos(\epsilon) \\ u_2 &= \frac{2}{\sqrt{6}}\sin(\frac{\pi}{6} - \epsilon) \\ u_3 &= \frac{2}{\sqrt{6}}\sin(\frac{\pi}{6} + \epsilon). \end{aligned} \tag{3.90}$$

On the caustic $\epsilon = 0$ which means that u_2 and u_3 in Eq. (3.90) coalesce. Outside of the caustic the method of steepest descents now involves only two path integrals. One through the complex point u_2 and the other going through the real stationary point u_1. The two paths must be able to cancel each other's contributions i.e., the must have the same magnitude but opposite signs. According to Kaminsky and Paris [8], from Eq .(3.65) the lowest order approximation for summing over two saddle point contributions gives the condition

$$\frac{e^{ix^2\psi(u_1)}}{\sqrt{6u_1^2 - 1}} + \frac{e^{ix^2\psi(u_2)}}{\sqrt{6u_2^2 - 1}} = 0. \tag{3.91}$$

Defining $d_1 = \sqrt{6u_1^2 - 1}$ and $d_2 e^{i\gamma} = \sqrt{6u_2^2 - 1}$, where the phase γ is the angle of $\sqrt{u_2^2 - 1}$ from the real axis. In addition, one can write.

$$\psi(u_2) = -\frac{1}{2}u_2^2 + \frac{3}{4}\frac{y}{x^{3/2}}u_2 = \psi_r + i\psi_i. \tag{3.92}$$

Restating Eq. (3.91) in terms of real and imaginary parts of ψ, one obtains

$$\frac{e^{ix^2\psi(u_1)}}{d_1} + \frac{e^{ix^2\psi_r - x^2\psi_i}}{d_2 e^{i\gamma}} = 0. \tag{3.93}$$

This equation can be split up into two separate pieces by looking at the modulus and phase of each term,

$$\begin{aligned} x^2\psi_i &= \log(\frac{d_1}{d_2}) \\ e^{ix^2\psi(u_1)} + e^{ix^2\psi_r - i\gamma} &= 0 \end{aligned} \tag{3.94}$$

with the second piece yielding,

$$x^2(\psi_r - \psi(u_1)) = (2j+1)\pi + \gamma \tag{3.95}$$

where $j = 0, 1, 2...$ is a non-negative integer as $|\psi(x,y)| > \psi(u_1)$ at all points outside of the caustic. Taking the ratio of the two equations for x^2 yields,

$$\log(\frac{d_1}{d_2})(\psi_r - \psi(u_1)) = ((2j+1)\pi + \gamma)\psi_i. \tag{3.96}$$

The stationary points u_1 and u_2 can be restated as $(\epsilon \to i\theta)$,

$$\begin{aligned} u_1 &= -\sqrt{\frac{2}{3}}\cosh\theta \\ u_2 &= \frac{1}{\sqrt{6}}\cosh\theta + \frac{i}{\sqrt{2}}\sinh\theta = u_3^* \\ 6u_2^2 &= \cosh^2\theta - 3\sinh^2\theta + i\sqrt{3}\sinh 2\theta, \end{aligned} \tag{3.97}$$

which can be further manipulated in order to obtain a useful factorised expression,

$$\begin{aligned} 6u_1^2 = d_1^2 &= 4\cosh^2\theta - 1 \\ &= 3\cosh^2\theta + \sinh^2\theta \equiv R^2 \end{aligned} \tag{3.98}$$

$$\begin{aligned} 6u_2^2 - 1 &= -2\sinh^2\theta + i\sqrt{3}\sinh 2\theta \\ &= 2i\sinh\theta(\sqrt{3}\cosh\theta + i\sinh\theta) \\ &= 2i\sinh\theta R e^{2i\gamma} = d_2^2 e^{2i\gamma}. \end{aligned} \tag{3.99}$$

A new term was introduced, R in Eq. (3.98), which is

$$\begin{aligned} R^2 = 3\cosh^2\theta + \sinh^2\theta &= \frac{\sinh 3\theta}{\sinh\theta} = (1 + 2\cosh 2\theta) \geq 3 \\ \tan 2\alpha &= \frac{\sinh\theta}{\sqrt{3}\cosh\theta} \end{aligned} \tag{3.100}$$

where $\gamma = \alpha + \frac{\pi}{4}$. In the first line of Eq. (3.99) the real component is negative and the imaginary component is a positive value, so the value is in the second quadrant. The square root will be in the first quadrant,

$$\begin{aligned} d_2^2 &= 2R\sinh\theta \\ &= 2\sqrt{\sinh\theta\sinh 3\theta} \approx \sqrt{12}\theta. \end{aligned} \tag{3.101}$$

Now that the d_2 parameter has been related to values for θ one can now deduce the locations of the nodes outside the caustic. So the next thing to do is to find an expression which can yield values for θ given an input for p. To start with note that $z_p = (2p + 1.25)\pi$.

Since Eq. (3.91) gives two expressions for x

$$\begin{aligned} x_a^2 &= \frac{2\sqrt{3}\log(d_1/d_2)}{(\cosh(3\theta) - \cosh(\theta))\sinh\theta} \\ x_b^2 &= \frac{2(z_j + \alpha)}{(\cosh(3\theta) + \cosh\theta)\cosh\theta - 0.5}. \end{aligned} \tag{3.102}$$

For consistency they should be the same, i.e. $x_a^2/x_b^2 = 1$. Therefore by taking the ratio of x_a^2/x_b^2 yields,

$$\frac{x_a^2}{x_b^2} = \frac{\sqrt{3}\log(d_1/d_2)}{(z_p + \alpha)}\frac{(\cosh(3\theta) + \cosh\theta)\cosh\theta - 0.5}{(\cosh(3\theta) - \cosh\theta)\sinh(\theta)} = 1, \tag{3.103}$$

which can be manipulated to produce

$$z_p + \alpha = \sqrt{3}\log(d_1/d_2)\frac{\cosh 2\theta\cosh^2\theta - 1/4}{\sinh 2\theta\sinh^2\theta}, \tag{3.104}$$

where

$$\begin{aligned} \frac{d_1}{d_2} &= \sqrt{\frac{R}{2\sinh\theta}} \\ R^2 &= 1 + 2\cosh 2\theta. \end{aligned} \tag{3.105}$$

Table 3.1 shows the first 10 positions and corresponding θ values for $p = 0, 1, 2..10$.

p	θ	x	y
0	0.460790	1.630894	2.400803
1	0.347758	2.984883	4.478403
2	0.302007	3.976072	6.211462
3	0.274735	4.796047	7.771618
4	0.255831	5.510953	9.220012
5	0.241609	6.152894	10.587300
6	0.230340	6.740457	11.891950
7	0.221083	7.285446	13.145970
8	0.213281	7.795825	14.357520
9	0.206568	8.277532	15.533120
10	0.200702	8.734851	16.677360

Table 3.1: Approximate locations of nodes

Fig. 3.8 shows the nodes from Table 3.1 with nodes inside and outside the caustic plotted. Label $p = 0, 1, 2 \ldots$ shows the family that the outside node belongs to. $p = 0$ has no node inside the cusp, $p = 1$ belongs to the family of one node $k = 0, j = 0$. $p = 2$ belongs to the family of two nodes $k = 1, j = 0$ and $k = 2, j = 0$ etc. Note how the further the nodes are from the origin the more bunched up the x and y values appear to be located.

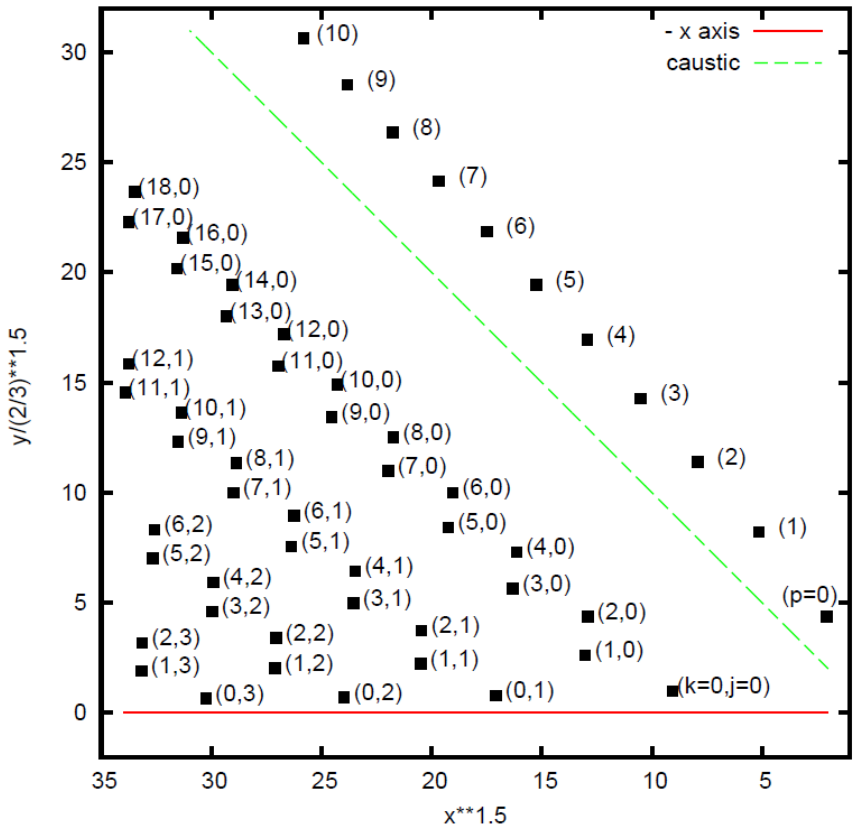

Figure 3.8: Location of 10 nodes outside the caustic.

Eq. (3.104) is of order $1/\theta^3$at small angles. Since the function is only needed over a small range of θ values, the Taylor series of the function can be used to deduce reasonable values for θ, $T(\theta) = z_p + \alpha, p = 0, 1, 2, \ldots$, and the nodal positions.

$$T(\theta) = \sqrt{3}\log(\frac{d_1}{d_2})\frac{\frac{1}{4}\cosh 4\theta + \frac{1}{2}\cosh 2\theta}{\frac{1}{4}\sinh 4\theta - \frac{1}{2}\sinh 2\theta}. \tag{3.106}$$

Eq. (3.106) has large cancellations in the denominator and might lead to problems. Therefore one looks at expansions in θ. Define the numerator and denominator by functions $N(\theta)$ and $D(\theta)$,

$$\begin{aligned} N(\theta) &= 0.75 + 3(\theta^2 + \theta^4) + \sum_{q=3}^{\infty} c_{2q}\theta^{2q} \\ D(\theta) &= 2(\theta^3 + \theta^5) + \sum_{q=3}^{\infty} d_{2q+1}\theta^{2q+1}, \end{aligned} \tag{3.107}$$

where $c_6 = 22/15$, $c_8 = 43/105$, $c_{10} = 38/525$, $c_{12} = 4/5$, $c_{14} = 10924/14189175$,$\cdots$, and $d_7 = 4/5$, $34/189$, $d_11 = 124/4725$, $d_{13} = 4/1485$, $\cdots$. The odd powers sum converges better than the even power. Taking the leading terms from Eq. (3.107) yields a truncated expressions

$$\begin{aligned} N_a(\theta) &\approx 0.75 + 3(\theta^2 + \phi^4) \\ D_a(\theta) &\approx 2(\theta^3 + \theta^5) \\ T_a(\theta) &= \frac{N_a(\theta)}{D_a(\theta)} \\ R^2 &\approx 3 + 4(\theta^2 + \frac{\theta^4}{3}). \end{aligned} \tag{3.108}$$

Using this truncated power expansion form of the equation the table of nodal positions can be reproduced to error in the fifth digit.

p	θ	x	y
0	0.46079	1.63089	2.40009
1	0.34776	2.98489	4.47841
2	0.30201	3.97607	6.21146
3	0.27474	4.79606	7.77163
4	0.25583	5.51095	9.22002
5	0.24161	6.51291	10.58735
6	0.23034	6.74047	11.89199
7	0.22108	7.728545	13.14598
8	0.21328	7.79585	14.35759
9	0.20657	8.27756	15.53319
10	0.20070	8.73484	16.67746

3.7 Number and density of nodes below caustic

Kaminsky and Paris gave a rough estimate for the location of the nodes, this can in turn be used to determine the accumulation of nodes as a function of x. One goes back to the Pearcey function in the form,

$$P(-x, y) = \sqrt{\frac{\pi}{x}} e^{-i\pi/4} \left(i\sqrt{2} e^{-x^2/4} \cos(y\sqrt{\frac{x}{2}} + 1 \right). \tag{3.109}$$

Separating into real and imaginary parts one obtains,

$$\begin{aligned} \cos(x^2/4)\cos(y\sqrt{x/2} &= 0 \\ \sin(x^2/4)\cos(y\sqrt{x/2}) &= -1/\sqrt{2}. \end{aligned} \tag{3.110}$$

The first line in Eq. (3.110) holds true if

$$x_p = 2\sqrt{(p + \frac{1}{2})\pi}. \tag{3.111}$$

In the trivial model each family of nodal points has p members at fixed position x_p and varying y_p. The second line of Eq. (3.110) reduces to,

$$y_{p,l} = \frac{2l-1}{4}\pi\sqrt{\frac{2}{x_p}}. \tag{3.112}$$

The cumulative number of nodes is,

$$N(p) = \frac{p(p+1)}{2} \tag{3.113}$$

Using Eq. (3.111) in terms of p and putting into the equation for the cumulative sum of nodes, one finds

$$\begin{aligned} 2N(p) &= \left(\frac{x_p^2}{4\pi} - \frac{1}{2}\right)^2 + \frac{x_p^2}{4\pi} - \frac{1}{2} \\ N(p) &= \frac{x_p^4}{32\pi^2} - \frac{1}{8} \end{aligned} \tag{3.114}$$

We will see later that the actual nodes differ in that x_p is not constant but rather x_p decreases as y_p increases. The trivial model is correct in that the nodes come in pairs.

However Eq. (3.114) underestimates the number of nodes. The main cause for this is that it does not consider the clustering of nodes as x_p is increased. The further you go from the origin the more closely packed the bands of nodes are, this causes the an additional number of nodes which is not predicted by this density function. An empirical formula can set up as

$$N(x) = a_v x^4 + a_s x^3. \tag{3.115}$$

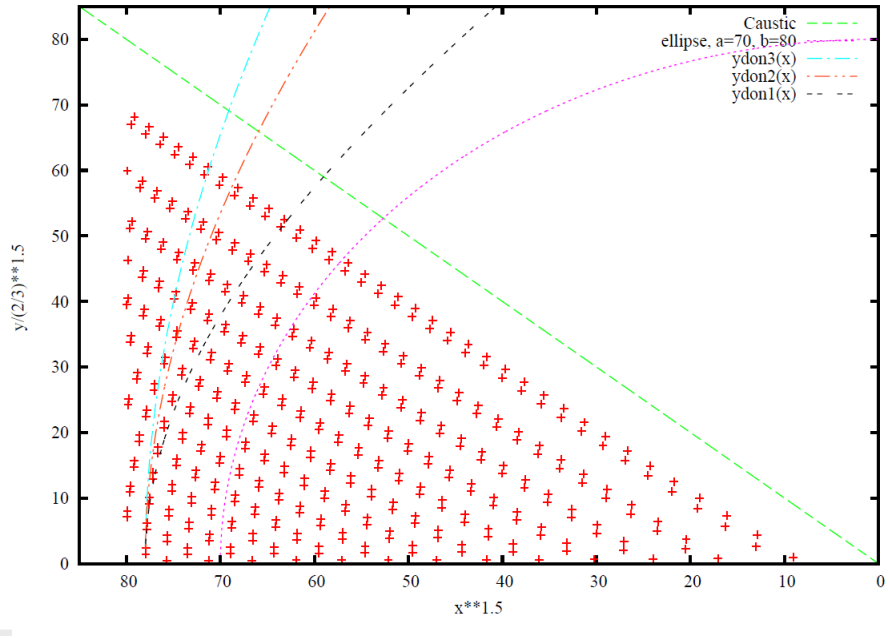

Figure 3.9: Approximately 400 nodes plotted vs $R = x^{3/2}$ and $\tilde{y} = y(3/2)^{3/2}$.

Fig 3.9 shows the positions of approximately 400 nodes. The curved lines are some guesses at circular or elliptical arcs that might better fit the curvature of the p-families. This choice of coordinates make evident that nodes of family labelled p occur roughly on circular arcs in $R, \tilde{y}$ plane. The family labelled by $p = 26$ occurs at $R = 78$, which is given by Eq. (3.111). The area is then $\pi R^2/8 \approx 2513$. The effective area is roughly 10% smaller as there is a gap between the nodes and caustic line which is empty of nodes. Problems arise as one moves further away from the origin. The family of p-nodes bends over, so much so in fact that the curvature is not parallel with other p-node arcs. Also the number of nodes in an area increases from the bending over of p-nodes families for larger x_p values. The causes the density to be slowly varying, the density measured for $R = 20$ is ≈ 0.064 and for $R = 80$ one finds ≈ 0.140, this is an increase of $\approx 100\%$. An illustrative attempt at lining up the arcs of p-nodes as an ellipse was also tried but the bending over of the nodes nearer the caustic varies too much for consistency. The trivial model predicts families of p-nodes which are perpendicular to R and therefore the calculations for density are erroneous as the curvature is not expected. The trivial model is sufficient for rough estimations of small x_p density calculations and does show that the nodes come in pairs, but for a robust method for calculating the density for large x_p it is not accurate enough.

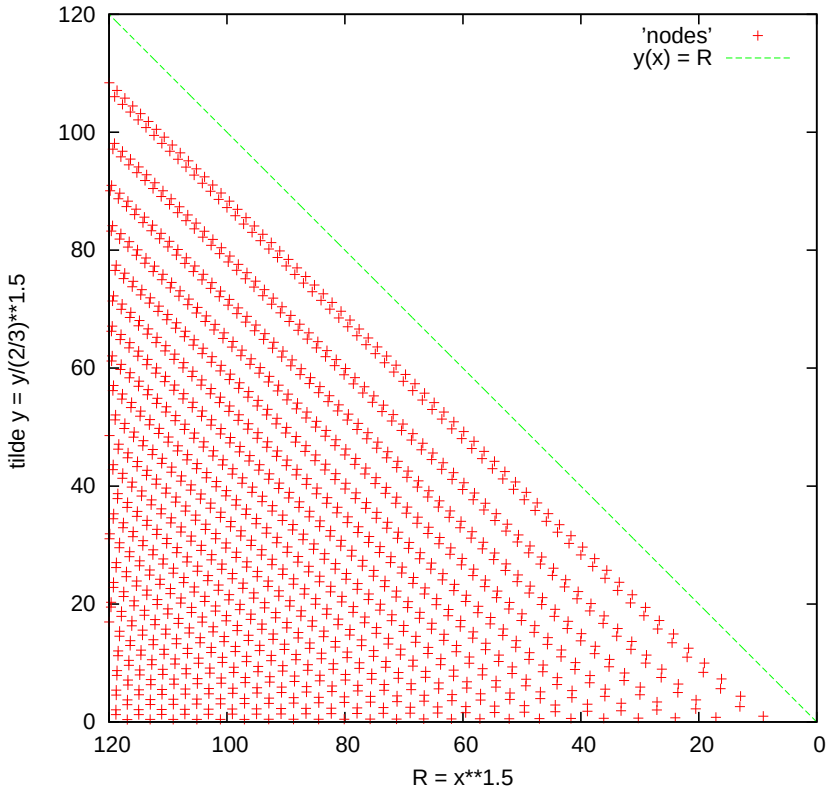

Figure 3.10: Approximately 1200 nodes plotted vs $R = x^{3/2}$ and $\tilde{y} = y(3/2)^{3/2}$.

Seen above in Fig. 3.10 are approximately 1200 nodes plotted inside the caustic. The coordinates R and $\tilde{y}$ have been chosen to show the caustic as a straight line running 45° to the R-axis. $R = 120$ corresponds to $x_p \approx 24$. One can use Eq. (3.111) to find the number of members belonging to the family $p = 46$. Eq. (3.113) predicts the number of nodes from the origin up to $R = 120$ to be $N \approx 1081$. Fig. 3.10 has around 1297 nodes, this is an excess of 20%. Lines for a p-family are perpendicular at the bottom but the curvature varies as y increases.

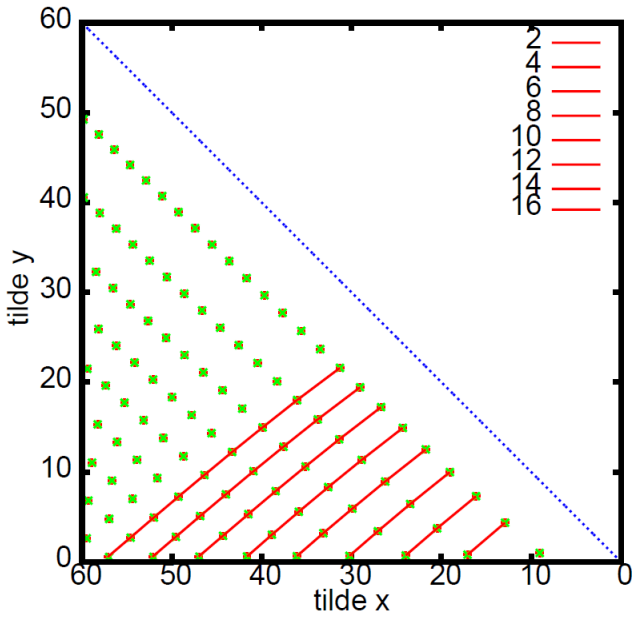

Figure 3.11: Nodes inside the caustic with modified axes $\tilde{x} = x^{3/2}$ and $\tilde{y} = y(3/2)^{3/2}$

Fig. 3.11 shows only upper nodes from the pairs for clarity. Fig. 3.11 highlights an alternative method of working out a way to find the density of nodes. The green nodes are running parallel to the caustic at $\theta = 45°$ to the horizontal. What is wanted are triangular sections with constant area inside the caustic to compute a uniform density of nodes. The red lines drawn are at 40° to the horizontal for small x but as one moves further to the left the angle decreases. This causes the area of the triangular sections to slowly change. Another problem with finding a constant density is due to the families of nodes not lying in straight lines. The bending over from the nodes closer to the caustic causes the density in the right-hand side portion of the triangular area to increase and the left-hand side to decrease.

Chapter 4

Conclusion

In this thesis we looked at approximate methods to locating nodes inside and outside of the caustic. Also the method of stationary phase was used to investigate $|P|$ around one of these points and its accuracy was examined. The method of stationary phase is used to find numerical values for $P(x, y)$ around a node. The equation for the curve of the stationary phase paths is found and a numerical integration recipe is applied in order to see the variation of the roots along the contour. One of the issues found was that there exists vertical segments along the contours of stationary phase paths but by using a Taylor series expansion in $y'(x)$ the problem is circumvented. By using the locations of nodes inside the caustic from calculations of the zeroth order approximation, the values of constant phase around a node are examined. Lines of constant $|P|$ are found to be slightly elliptical around a node which is expected from the $|P|$ plot the figure A.1 found in Stamnes and Spjelkavik. [1] . Accuracy for $|P(x, y)|$ to 10^{-8} digits is found, beyond that $|P|$ values fluctuate too much. Approximate locations of the nodes outside the caustic are obtained from the lowest order approximation Eq. (3.91) and plotted in Fig. 3.8. The nodes outside the cusp run parallel to the caustic. They also differ from the ones inside the cusp as the they do not appear to come in pairs. The density of nodes is found to be slowly varying. This is due to the fact that the lowest order approximations expect the family of nodes be found in vertical columns perpendicular to the x-axis. It is instead found from numerical calculations that the family of nodes are slightly elliptical and have a varying curvature. An empirical formula for the density of nodes is found but no exact forms for the density of nodes is obtained.

An interesting topic which was untouched here is the investigation into the bright spots inside a cusp. The bright spots are seen in Stamnes' and Spjelkaviks' paper [1] in the plot of $|P|$, see appendix A. They are the hill-tops of $|P|$, whereas what we have looked at are the nodes which correspond to the valleys of $|P|$. The hill-tops of $|P|$ corresponds to the unstable surface in Fig. 2.3. This project has focused

on one topic in short-wavelength phenomena and reasonable accuracy of the nodes inside the caustic has been found but improvements could be made. Higher order approximations or analytical solutions of the Pearcey function would yield a more accurate map of nodes.

Bibliography

[1] J.J. Stamnes and B. Spielkavik. Evaluation on the field near a cusp of a caustic. *Optica Acta*, 30:1331–1358, 1983.

[2] T. Pearcey. Structure of an electromagnetic field in the neighbourhood of a cusp of a caustic. *Phil. Mag.*, 37:311–317, 1946.

[3] Tamás Kalmár-Nagy Russell Trahan. Equilibrium, stability and dynamics of rectangular liquid-filled vessels. *J.Comput Nonlinear Dynam(6)4*, 15, 2011.

[4] M. V. Berry. Cusped rainbows and incoherence effects in the rippling-mirror model for particle scattering from surfaces. *J.Phys. A 8*, pages 566–584, 1975.

[5] J.N.L. Connor. Theory of cusped rainbows in elastic scattering: Uniform semi-classical calculations using pearcey integral. 1980.

[6] N. M. Maslin. Caustics and cusps in an isotropic ionosphere. *J. Atmos. Terr. Phys*, 38:239–250, 1976.

[7] A. Mourka M. Mazilu K. Dholakia M.R. Dennis J.D. Ring, J. Lindberg. Auto-focusing and self-healing of pearcey beams. *Optical Society of America*, 2012.

[8] D. Kaminski and R.B. Paris. On the zeroes of the pearcey integral. *J. Computational and Applied Mathematics*, 107:31–52, 1990.

[9] R. Thom. Stabilité structurelle et morphogenése. *Inter Editions*, 1972..1977.

[10] T. Poston and I. Stewart. "catastrophe theory and its applications". , pages 246–249, 1978.

[11] E.C. Zeeman. A catastrophe machine. *Towards a Theoretical Biology 4. Essays, ed*, pages 276–282, 1972.

[12] P. T. Saunders. *An introduction to catastrophe theory.* Cambridge University Press, 1980.

[13] George Arfken. *Mathematical Methods for Physicists.* Academic Press, INC, Orlando, Florida, third edition, 1985.

[14] N. Bleistein and R. A. Handelsman. *Asymptotic Expansions Of Integrals*. Cambridge University Press, first, 1975 edition, 1975.

[15] W.T. Vetterling W.H. Press, S.A. Teukolsky and B.P. Flannery. *Numerical Recipes in Fortran*. Cambridge University Press, Cambridge U.K., second, 1992 edition, 1992.

Appendix A

Plots of $|P|$ and phase P from Stamnes and Spjelkavik [1]

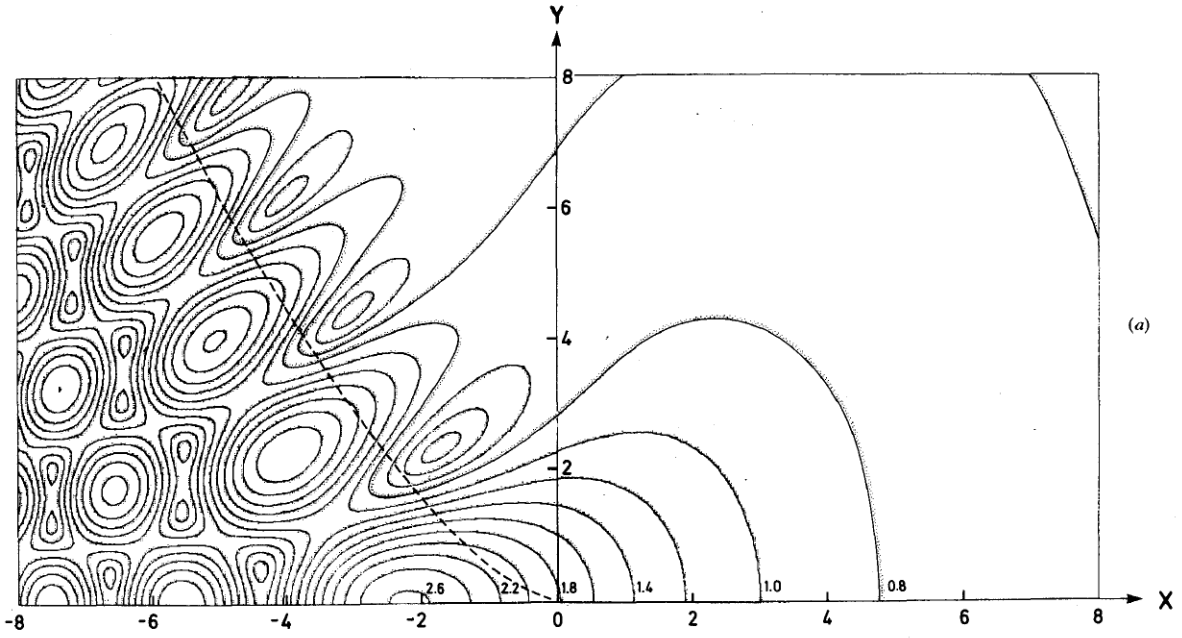

Figure A.1: Contour lines of constant $|P(x,y)|$ of the Pearcey function. The dashed curve is the caustic. $|P(x,y)|$ has a maximum value of 2.64 at $x \approx -2.2$, $y = 0$. The contour lines are separated by equal intervals of 0.2, and the dotted side of each contour line indicates the direction of descent.

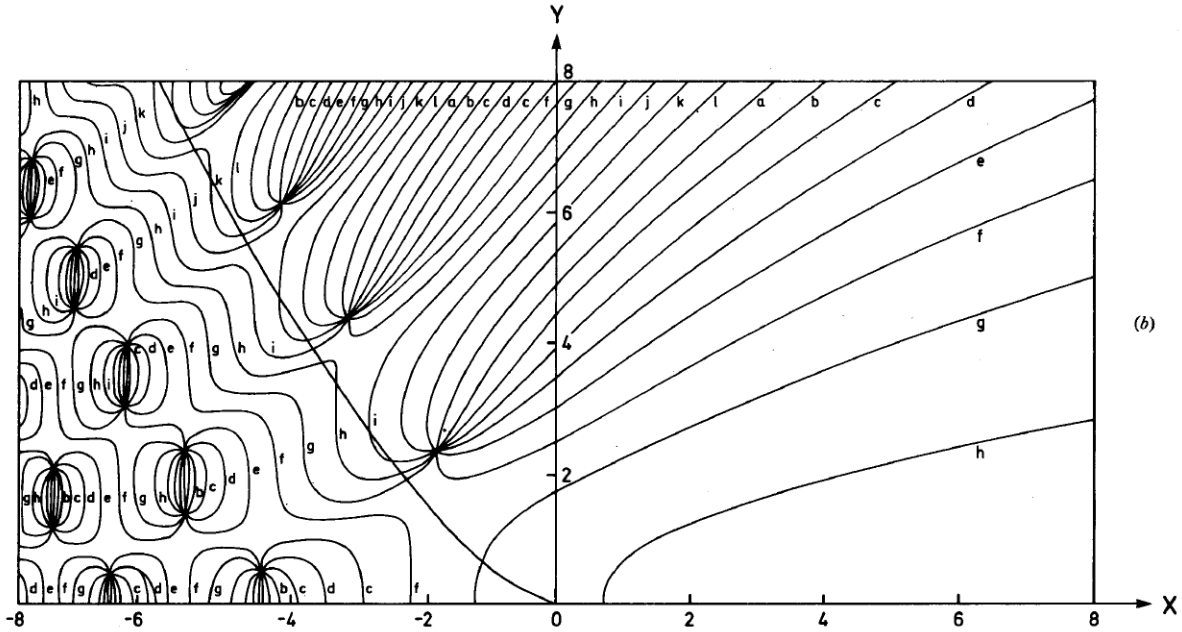

Figure A.2: Contour lines of constant phase of the Pearcey function $P(x,y)$. The dashed curve is the caustic. The contours are labelled $a = \pm 180°$ and from $b = -150°$ to $l = 150°$ in steps of 30°.